

KSHV Episome Tethering Sites on Host Chromosomes: Regulation of Latency-Lytic Switch by the ChAHP complex

Ashish Kumar

UC Davis School of Medicine

Yuanzhi Lyu

UC Davis School of Medicine

Yuichi Yanagihashi

Lifematics

Chanikarn Chantarasrivong

Lifematics

Vladimir Majerciak

National Cancer Institute <https://orcid.org/0000-0003-2907-4583>

Michelle Salemi

University of California, Davis

Kang-Hsin Wang

UC Davis

Frank Chuang

UC Davis

Ryan Davis

UC Davis <https://orcid.org/0000-0001-7439-6683>

Clifford Tepper

UC Davis <https://orcid.org/0000-0001-7105-1102>

Kazushi Nakano

Lifematics

Chie Izumiya

UC Davis

Michiko Shimoda

UC Davis

Ken-ichi Nakajima

UC Davis

Alexander Merleev

UC Davis

Zhi-Ming Zheng

Tumor Virus RNA Biology Section, HIV Dynamics and Replication Program, Center for Cancer Research,
National Cancer Institute, National Institutes of Health, Frederick, MD 21702, USA

Mel Campbell

UC Davis <https://orcid.org/0000-0002-8475-6686>

Yoshihiro Izumiya (✉ YIZUMIYA@UCDAVIS.EDU)

UC Davis School of Medicine <https://orcid.org/0000-0002-9184-2603>

Article

Keywords: LANA, ChAHP, KSHV, Episome Tethering Sites

Posted Date: September 22nd, 2021

DOI: <https://doi.org/10.21203/rs.3.rs-136834/v2>

License:  This work is licensed under a Creative Commons Attribution 4.0 International License.

[Read Full License](#)

1 **KSHV Episome Tethering Sites on Host Chromosomes: Regulation of**
2 **Latency-Lytic Switch by the ChAHP complex**

3
4 Ashish Kumar^{1, #}, Yuanzhi Lyu^{1, #}, Yuichi Yanagihashi^{2, #}, Chanikarn Chantarasrivong²,
5 Vladimir Majerciak³, Michelle Salemi⁴, Kang-Hsin Wang¹, Frank Chuang⁵, Ryan R. Davis⁶, Clifford G.
6 Tepper^{5, 7}, Kazushi Nakano², Chie Izumiya¹, Michiko Shimoda^{1, 7}, Ken-ichi Nakajima¹,
7 Alexander Merleev¹, Zhi-Ming Zheng³, Mel Campbell^{1,*}, & Yoshihiro Izumiya^{1,5,7,*}
8

9 ¹ Department of Dermatology School of Medicine, University of California Davis (UC Davis), Sacramento,
10 California USA

11 ² Lifescience Division, Lifematics, Osaka, 541-0046 Japan

12 ³ HIV Dynamic and Replication Program, National Cancer Institute, NIH, Frederick, Maryland, USA

13 ⁴ Genome Center, Proteomics Core, Genome and Biomedical Sciences Facility, UC Davis, Davis, California,
14 USA

15 ⁵ Department of Biochemistry and Molecular Medicine, School of Medicine, UC Davis, Sacramento,
16 California USA

17 ⁶ Department of Pathology and Laboratory Medicine, School of Medicine, UC Davis, Sacramento, California
18 USA

19 ⁷ Viral Oncology and Pathogen-Associated Malignancies Initiative, UC Davis Comprehensive Cancer Center,
20 Sacramento, California USA

22 # These authors contributed equally.

23
24
25 * Correspondence: Mel Campbell, PhD
26 Address: UCDMC Research III, Room 3300D, 4645 2nd Avenue, Sacramento CA 95817
27 E. mail: mcampbell@ucdavis.edu
28 Phone: 916-734-7811

29
30 *Correspondence: Yoshihiro Izumiya DVM, PhD
31 Address: UCDMC Research III, Room 2200B, 4645 2nd Avenue, Sacramento CA 95817
32 E. mail: yizumiya@ucdavis.edu
33 Phone: 916-734-7253

36 Word counts:

37 Abstract: 150

39 **Abstract**

40 Kaposi's sarcoma-associated herpesvirus (KSHV) establishes a latent infection in the cell
41 nucleus, but where KSHV episomal genomes are tethered and the mechanisms underlying
42 KSHV lytic reactivation are unclear. Here, we study the nuclear microenvironment of KSHV
43 episomes and show that the KSHV latency-lytic replication switch is regulated via viral long non-
44 coding (lnc)RNA-CHD4 (chromodomain helicase DNA binding protein 4) interaction. KSHV
45 episomes localize with a CHD4 complex, ChAHP, at epigenetically active genomic regions and
46 tethers frequently near centromeric regions of host chromosomes. The ChAHP complex also
47 occupies the 5'-region of a highly-inducible lncRNAs and terminal repeats of KSHV genome with
48 latency-associated nuclear antigen (LANA). Viral lncRNA binding competes with CHD4 DNA
49 binding, and KSHV reactivation is accompanied by the detachment of KSHV episomes from host
50 chromosome docking sites. We propose a model in which elevated lncRNA expression
51 determines the KSHV latency-lytic decision by regulating LANA/ChAHP DNA binding at
52 inducible viral enhancers.

53

54 **Introduction**

55 Kaposi's sarcoma-associated herpesvirus (KSHV), discovered in 1994, is one of eight human
56 herpesviruses (1). Since then, KSHV has been identified as the causative agent of Kaposi's
57 sarcoma (1-3) and two human lymphoproliferative diseases, primary effusion lymphoma (PEL)
58 and AIDS-related multicentric Castleman's disease (4-7). Although HAART (highly active
59 antiretroviral therapy) of HIV-patients dramatically reduced KS incidence in Western countries,
60 KSHV associated-malignancies are still a leading cause of cancer deaths in AIDS patients in
61 Sub-Saharan Africa. Additional therapeutic measures are urgently needed. In cancer cells,
62 KSHV establishes a latent infection in which most viral genes are silenced with the exception of
63 few latent proteins, such as latency associated nuclear antigen (LANA) (8). External stimuli
64 trigger KSHV reactivation in latently infected cells through activation of highly potent viral
65 transactivator, K-Rta, which then activates early gene expression including three viral long non-
66 coding RNAs (9-11).

67 KSHV LANA is a 130 kDa multifunctional protein, which plays a major role in both DNA
68 replication and episome maintenance during latency. LANA binds DNA sequences within the
69 801 base pair terminal repeats (TRs) of the KSHV genome, which serve as both an origin of
70 DNA replication and a site for tethering episomes to the host cell chromosomes (12-15). There
71 are two distinct mechanisms through which LANA tethers episomes to host cell chromosomes.
72 First, the N-terminus of LANA, which is predicted to be highly-unstructured, can interact with
73 host chromosomes through direct binding with histone H2A and H2B (16, 17). A second
74 mechanism involves the interaction of the LANA DNA binding domain (DBD) with host
75 chromatin-associated proteins (18-20). The chromatin-associated proteins include BRD2 and
76 BRD4, which contain two bromodomains that recognize the acetylated H3 and H4 histones, and

77 a conserved C-terminal extraterminal domain (21, 22). The BRD extraterminal domain interacts
78 directly with the LANA DBD, providing a putative mechanism for episome docking sites selection
79 at epigenetically active host chromosomes (18, 23). In both mechanisms, tethering requires a
80 sequence-specific interaction between the LANA DBD and the viral episome at LANA binding
81 sites 1 and 2 (LBS 1/2) (15). Episome maintenance requires at least two copies of LBS1/2 and
82 the KSHV genome encodes 30 to 40 terminal repeats, taking up to approximately one fifth of
83 KSHV genome (24-32 kbp DNA fragment) (24). The crystal structures of the LANA DBD further
84 revealed that LANA can form a higher-order decameric ring structure, and a hydrophobic
85 interface between LANA dimers to form the decameric ring is important for cooperative LBS1/2
86 binding, DNA replication, and thereof episome maintenance (25). The crystal structure of LANA
87 DBD also reveals distinct binding interfaces among BRD2/4 binding site, DNA binding, and
88 decameric interfaces (25, 26).

89 Spatial and temporal organization of the genome plays a critical role in gene expression
90 in many organisms including large DNA viruses (27, 28). Similar to cellular genes, the KSHV
91 episome changes its genomic structure with increasing genomic looping at KSHV Replication
92 and Transactivation (K-Rta) binding sites during KSHV reactivation (28). Imaging studies
93 suggested that DNA/RNA/protein aggregates are formed at actively transcribed sites, in which
94 a significant fraction of RNA Polymerase II (RNAPII) is recruited to the KSHV genomes and used
95 to transcribe viral genomes during KSHV reactivation (29). Such transcription factory formation
96 is known to bring gene promoters and enhancers together (27). It is clear that dynamic regulation
97 of genome architecture plays a critical role in gene transcription, hence outcomes of KSHV
98 latency-lytic replication decisions. However, the mechanisms that control KSHV episome
99 architecture remains elusive.

100 Chromatin remodeling enzymes have been of wide interest in the regulation of KSHV
101 latency-lytic switch. The enzymes include polycomb repressor complex 1 and 2, nucleosome
102 remodeling and deacetylase (NuRD), lysine demethylases (KDM2B, 3A, and 4A), histone lysine
103 acetylase and methylases (20, 30-35). Recent studies highlight that chromatin remodeling
104 enzymes also participate in regulation of genome architecture. In murine embryonic stem cells,
105 the Iswi family remodeler Snf2h promotes CTCF binding to the genome and regulates formation
106 of contact domains (36, 37). In addition to Snf2h, CHD4 (chromo domain helicase DNA binding
107 protein 4) has recently been shown to occupy and restrict enhancer accessibility as well as
108 cohesin occupancy at CHD4 binding sites (38). Genetic disruption of CHD4 therefore causes
109 spontaneous differentiation concomitant with premature activation of lineage-specific genes (39-
110 41). CHD4 has been identified in two distinct cellular protein complexes, the NuRD and ChAHP
111 complexes (42). The ChAHP complex consists of CHD4, ADNP (activity-dependent
112 neuroprotective protein), and HP1 γ (heterochromatin protein 1) (39). ADNP binds DNA
113 sequence motifs such as *GCCCTCTTCTGG* and anchors the ChAHP complex to euchromatin
114 (43). ChAHP complex was shown to modulate spatial chromatin loop organization locally, and
115 counteract chromatin looping at CTCF sites (43). Accordingly, ChAHP plays essential roles in
116 maintaining distinct cellular states and ensure accurate cell fate decisions in response to external
117 signals during development that are likely to associate with its function in regulation of enhancer
118 accessibility (39, 41, 44). Because of CHD4's roles in enhancer regulation, it is not surprising
119 that mutation or overexpression of CHD4 has been linked to multiple developmental disorders
120 and malignancies in humans (45-48).

121 The long non-coding (lnc)RNAs that are transcribed from active enhancers in a cell- or
122 tissue- specific manner are called enhancer RNAs (eRNAs) (49). The functions of eRNAs are

123 largely mediated through interactions with eRNA binding partners (50-52); however, studies also
124 indicated that RNA sequence is not contributing to the specificity of eRNA-protein interactions.
125 Instead, specificity of the function is suggested to be achieved through gene/RNA positioning
126 and spatial proximity to regulated genomic regions (53). Similarly, the KSHV genome encodes
127 at least three highly inducible lncRNAs (Ori-RNA [also called T1.5], Poly Adenylated Nuclear
128 RNA [PAN RNA], and T0.7) that are transcribed from epigenetically active regions, and are direct
129 targets of K-Rta (11). The PAN RNA genomic locus actively recruits cellular RNAPII during
130 KSHV reactivation, leading to significantly higher copy number of PAN RNA molecules (up to
131 10^5 copies) in a reactivating cell (54). The high copy number of PAN RNA has also been
132 explained by its higher RNA stability (55). Three sequence elements, ENE (expression and
133 nuclear retention element) at the 3' region, MRE (Mta responsive element) at the 5' region of
134 PAN RNA, and the structure of the poly (A) tail, are critical for PAN RNA stability (56-58). PAN
135 RNA interacts with multiple cellular and viral proteins (57, 59), and functions as a transactivator
136 by sequestering repressors and/or recruiting histone modifying enzymes (32, 60, 61). A recent
137 report shows that PAN RNA could be replaced by other viral lncRNA sequences without a
138 significant loss of KSHV replication, suggesting that there is a sequence-independent function
139 similar to that of eRNAs (62).

140 In this study, we provide evidence that the KSHV latent-lytic switch is regulated by the
141 ChAHP complex. We mapped KSHV episome tethering sites on host chromosomes with
142 Capture Hi-C and studied the surrounding nuclear microenvironment of KSHV episomes using
143 proximity biotin labeling. We show that KSHV episomes co-localize with the ChAHP complex at
144 epigenetically active host chromosomes, and CHD4 interaction with viral lncRNAs regulates
145 binding of CHD4 on KSHV chromosomes, which de-represses viral lncRNAs from ChAHP-

146 mediated repression. We propose that the inducible enhancer activity is regulated by a balance
147 between local eRNA transcription activity and ChAHP complex tethering, and the mechanism
148 regulates KSHV reactivation.

149

150 **Results**

151 **Identification of KSHV episome tethering site on host chromosomes.**

152 KSHV episomes tether to the host cell chromosomes via LANA, however the mechanism of
153 selection of docking sites is not very well characterized. To understand how and where KSHV
154 episomes tether to host chromosomes, we applied Capture Hi-C (CHi-C) method to identify
155 episome docking sites in three KSHV naturally-infected PEL cell lines, BC-1, BC-3 and BCBL-
156 1. The schematic diagram for the CHi-C procedure is presented in **Fig. 1a**. In order to obtain
157 high resolution, the Hi-C sequencing library was further enriched by using biotinylated tiling-oligo
158 probes that specifically hybridized to KSHV DNA sequences (**Fig. 1a**). Using this method, we
159 examined the position of host genomic regions that exhibited higher frequencies of normalized
160 chimeric ligation reads with KSHV DNA fragments. We identified selectively enriched chimeric
161 ligation reads throughout the host chromosomes (**Fig. 1b**). The mapped reads on 23 individual
162 chromosomes for BC-1, BC-3 and BCBL-1 are presented separately in **Supplementary Fig. 1a-**
163 **c**. Each dot represents the number of normalized contact heterotypic sequence reads between
164 host and KSHV sequences. The CHi-C normalized chimeric read counts on chromosome 1 for
165 three naturally infected PEL cells are shown in **Fig. 1c**. The results indicated that there are a
166 higher number of chimeric read counts near centromeric regions in all three cell lines (**Fig. 1c**).
167 To study the frequencies of chimeric read counts that are located near the centromere region,

168 we performed a mathematic characterization, in which we extracted the chimeric read counts
169 that derived from regions spanning a distance corresponding to 1% of the size of each
170 chromosome at either 5' or 3' centromere chromosome regions (marked green and blue). Counts
171 per 100 kbp were calculated separately for each chromosome and compared to the average
172 number across the individual chromosome. The results showed that higher chimeric read counts
173 were seen (15 out of 23 chromosomes in BCBL-1) either 5' or 3' regions of centromere, and in
174 some instances (e.g., chromosome 8, 19, X), we observed enrichment in both 5' and 3' positions
175 (**Fig. 1d**). To further confirm the CHi-C findings, we performed DNA-FISH with centromere-
176 specific PNA (peptide nucleic acid) probes in combination with LANA immunostaining. These
177 results further showed that a large fraction of LANA dots was colocalized with centromeres (**Fig.**
178 **1e, Supplementary Fig. 2**). The results are consistent with a previous report, which
179 demonstrated that LANA colocalized with centromeric protein F (CENPF) and kinetochore
180 protein, Bub1, and observed at centromere regions during metaphase (63). To determine
181 whether KSHV docking sites are random, we next examined the similarity of KSHV episome
182 tethering sites among the three cell lines using a Jaccard Index. We calculated the similarity of
183 tethering sites based on the positions of chimeric sequence reads. The index identified 97.86%
184 (BC-1 vs BC-3), 81.99% (BC-1 vs BCBL-1) and 82.36% (BC-3 vs BCBL-1) similarity (**Fig. 1f**).
185 The results demonstrated that a majority of KSHV episomes tethers the similar host genomic
186 regions in three naturally infected PEL cell lines, suggesting that there is a preferential nuclear
187 microenvironment that can attract/maintain KSHV latent episomes during cell divisions.
188

189 **Identification of proteins in close proximity to KSHV latency associated nuclear antigen**
190 **(LANA).**

191 Next, we examined the nuclear protein microenvironment of KSHV episome-tethering sites in
192 infected cells. We hypothesized that, by examining cellular proteins neighboring to LANA in
193 infected cells, we should be able to identify the repertoire of proteins important for tethering and
194 selection of KSHV episome-docking sites. To identify proteins in close proximity to LANA, we
195 used a miniTurbold based method. The miniTurbold is a biotin ligase, which covalently attaches
196 biotin to lysine residues in neighboring proteins (<10 nm) in less than 10 minutes with no
197 significant cell toxicity (64, 65). A recombinant KSHV BAC16 with LANA N-terminal tagged with
198 miniTurbold (referred to as KSHV LANA-mTID) was prepared; the procedure for the preparation
199 of KSHV LANA-mTID is presented in **Supplementary Fig. 3**. We transfected the *i*SLK cells with
200 the recombinant KSHV LANA-mTID and stably selected with hygromycin (1 mg/ml). The KSHV
201 LANA-mTID virus was then recovered by inducing reactivation with doxycycline (1 µg/ml) and
202 sodium butyrate (3 mM) for 5 days. *i*SLK cell line was infected with recombinant KSHV LANA-
203 mTID virus and selected with hygromycin (1 mg/ml) to generate stable *i*SLK-LANA mTID cells
204 (**Fig. 2a**). The *i*SLK-LANA mTID cells were incubated with D-biotin for 60 minutes in culture
205 media and biological triplicated samples were prepared (**Fig. 2b**). This strategy led us to identify
206 76 host proteins ($P<0.05$) that were physically neighboring KSHV LANA within 10 nm radial
207 distance during the period of D-biotin incubation (64). The 76-host proteins include nuclear
208 mitotic apparatus protein (NuMA), bromodomain-containing protein 4 (BRD4), and lysine-
209 specific demethylase 3A and 3B (KDM3A and 3B) that have been previously shown to physically
210 interact with LANA (20, 66-68) (**Fig. 2c, Supplementary Table 1**). In addition to those previously
211 identified cellular proteins, the study also precipitated components of the ChAHP complex (39),
212 which is composed of chromodomain helicase DNA-binding protein 4 (CHD4), Activity-
213 dependent neuroprotector homeobox protein (ADNP) and HP-1γ with high confidence (**Fig. 2c**).

214 Although we could not identify HP-1y with our statistical criterion in proteomics study, HP-1y
215 protein was previously shown to interact with KSHV LANA (69). The LANA interaction with CHD4
216 and ADNP was further validated with *in vitro* pull-down assays, and the results showed that
217 LANA could interact with CHD4 and ADNP in the absence of other viral proteins (**Fig. 2d**).
218 Further, recombinant GST-tagged LANA deletion proteins (**Supplementary Fig. 4**) were used
219 to map the interaction domain with CHD4 and found that the amino acid (aa) residues 870-1070,
220 near the LANA DNA-binding domain, were responsible for interaction with CHD4 (**Fig. 2e**).
221 Immunofluorescence assays with mono-specific antibodies further confirmed that LANA and
222 CHD4 were colocalized in naturally infected BCBL-1 cells (**Fig. 2f**). Taken together, these results
223 suggest that LANA is able to associate with the ChAHP complex in latently infected cells.

224

225 **Association of KSHV episome-tethering sites with ChAHP complex binding.**

226 The protein interaction and colocalization between CHD4 and LANA "dots" in the nucleus led us
227 to further investigate the localization of CHD4, ADNP and LANA on both host and KSHV
228 chromosomes. To identify the chromatin occupancy site(s) for ChAHP complex and LANA, we
229 employed Cleavage Under Targets and Release Using Nuclease (CUT&RUN) (70). The LANA,
230 CHD4, and ADNP CUT&RUN peaks clearly overlapped at multiple sites of cell host
231 chromosomes with active histone marks (H3K27Ac), which include previously described IRF4
232 super enhancer region (71, 72) (**Fig. 3a**). NGS plots between LANA CUT&RUN summit peaks,
233 and CHD4 or ADNP further confirmed co-occupancies of LANA and the ChAHP complex on the
234 host chromosomes (**Fig. 3b**). Because LANA and ChAHP complex interact with each other, we
235 hypothesized that LANA-ChAHP complex could be important for tethering KSHV episomes to
236 host chromosomes. To test this, we generated NGS plots between LANA, CHD4 and ADNP

237 CUT&RUN summit peaks, and distribution of CHi-C chimeric reads. We observed that KSHV
238 episome tethering sites were indeed primarily localized near the LANA, CHD4 and ADNP binding
239 sites, whereas it was not observed for H3K4me1 (**Fig. 3c**) or H3K27me3 (**data not shown**). To
240 further calculate degree of interaction mathematically, we measured the relative CHi-C chimeric
241 reads per million and examined association with relative distance with CHD4 binding site.
242 Accumulation index calculated from NGS plot suggested that more than 50% of CHi-C reads are
243 closely located at CHD4 binding site within the genomic regions (**Fig. 3d**). Altogether, these
244 results suggest that KSHV episome tethers to host chromosome at the ChAHP binding sites.

245

246 **KSHV LANA colocalization with ChAHP complex on KSHV genome.**

247 We next examined ChAHP binding sites on the KSHV episome. Consistent with studies with
248 cellular chromosomes, CHD4 and ADNP occupy genomic loci with active histone marks, which
249 includes KSHV long non-coding RNAs (PAN RNA, T0.7, and T1.5 [Ori-RNA]) promoter regions
250 (**Fig. 4a**). The results also showed colocalization among LANA, CHD4, and ADNP with the active
251 histone mark, H3K27Ac, along the KSHV genome, and exceptionally strong peaks were seen at
252 terminal repeat regions (read counts are depicted in Fig. 4a), where multiple copies of LANA
253 bind (73). The strong peaks at TR regions are likely due to a combination of tighter binding of
254 the complex and the presence of multiple copies of the same sequences. The strong signals at
255 TR regions are unlikely due to mapping problems, because H3K27me3 showed a lower number
256 of sequence reads compared with sequence reads in the unique region. The three viral lncRNAs,
257 especially PAN RNA, are known to be expressed at significantly higher transcript copy numbers
258 than the open reading frames during lytic replication (54, 74), and CHD4, ADNP, and LANA were
259 clearly localized at the 5' regions of these lncRNA promoter regions (**Fig. 4a**). Next, the effects

260 of KSHV reactivation on CHD4 occupancies were examined by CUT&RUN with qPCR. The
261 results suggested that CHD4 occupancies on the KSHV genome were reduced during KSHV
262 reactivation (**Fig. 4b**). We further studied effects of KSHV reactivation on the KSHV episome
263 tethering with the ChAHP complex on host cell chromosomes. For this, TREx-BCBL-1 cells were
264 reactivated for twenty-four hours and CHi-C samples were prepared. We measured the relative
265 chimeric DNA sequence frequencies of KSHV with host chromosomes before and after KSHV
266 reactivation. The relative amount of chimeric sequence reads at one of the KSHV episome
267 tethering sites were visualized with Juicebox. By subtracting the number of relative sequence
268 reads in latent samples from those in reactivated samples, we also visualized changes by
269 induction of active viral transcription. The results showed that KSHV chimeric sequence reads
270 were reduced, suggesting that KSHV reactivation induced detachment of the KSHV episome
271 from host chromosomes, and a similar detachment was also seen in other putative episome-
272 tethering sites (**Fig. 4c**). The results suggest that robust viral lncRNAs at the ChAHP binding site
273 may play a role in detachment of ChAHP/LANA complex from chromosomes.

274

275 **Identification of PAN RNA binding proteins with proximity biotinylation.**

276 Previous studies including ours suggested that PAN RNA transcription *in cis* plays an essential
277 role in initiation of KSHV lytic replication. Inhibition of PAN RNA transcription by either deletion
278 of the PAN RNA sequence or mutation at K-Rta responsive elements in the PAN RNA promoter
279 significantly impaired KSHV reactivation and replication (28, 60). In addition, CHD4 is known to
280 bind cellular enhancers to regulate enhancer-promoter interactions, and enhancers often
281 transcribed enhancer RNAs (lncRNAs) (75). To examine PAN RNA-mediated transcription
282 regulation, we again applied the proximity labeling technique to profile PAN RNA neighboring

283 proteins during KSHV reactivation. This time, the mTID cassette was first inserted as an N-
284 terminal fusion of ORF57, a PAN RNA binding protein, and then the fusion protein was
285 expressed from the endogenous promoter during KSHV reactivation (**Fig. 5a**). Taking advantage
286 of a previous detailed mapping study, which identified ORF57 binding sites on PAN RNA, termed
287 MRE (Mta Responsive Element) (57), we utilized a PAN MRE mutant virus having a 9-nucleotide
288 mutation in the MRE element (**Fig. 5a**). KSHV genome-wide qRT-PCR array analysis confirmed
289 previous studies that the PAN RNA MRE mutation impaired viral gene expression, with stronger
290 effects being seen in late gene cluster regions (**Supplementary Fig. 5a right panel**). We also
291 confirmed that protein biotinylation happened only in the presence of both ORF57 protein
292 (reactivated sample) and biotin (**Fig. 5b**). By comparing the enrichment profiling between the
293 PAN RNA MRE mutant and PAN RNA Wt, we isolated cellular proteins that are in proximity to
294 ORF57 protein via PAN RNA binding. Proximity biotin labeling identified a total of 129 and 307
295 proteins from mTID-57 PAN Wt *iSLK* cells and mTID-57 PAN-MRE *iSLK* cells, respectively
296 ($p < 0.05$) (**Supplementary Table 2**). Among the interacting proteins, 74 proteins were common
297 between the PAN MRE Wt and PAN MRE mutant, while 55 proteins were found only in the
298 presence of the wild type PAN RNA sequence (**Fig. 5c, d**). Deletion of MRE seemed to unleash
299 ORF57 protein and allow ORF57 to interact more freely with other RNA binding proteins (**Fig.**
300 **5c**). Importantly, this proteomics approach identified CHD4 as a putative PAN RNA binding
301 protein ($p < 0.005$). Next, we performed the siRNA screening of 129 (55 + 74) PAN RNA binding
302 proteins with KSHV reactivation indicator cell line, *iSLK.219*. The knockdown screening identified
303 4 strong repressors namely IK, CHD4, PABPC3 and RPL18A with fold change (RFP/GFP) > 3
304 among the 129 proteins, and CHD4 was found be the strongest among them (RFP/GFP > 7 -
305 fold) (**Fig. 5e**). Gene Ontology (GO) analysis of 129 PAN RNA-mediated ORF57-interacting

306 proteins suggested that ORF57 is indeed primarily involved in RNA processing (**Supplementary**
307 **Fig. 5b).**

308

309 **A viral lncRNA inhibits CHD4 dsDNA binding.**

310 PAN RNA MRE-dependent enrichment by ORF57-mediated biotinylation suggested that CHD4
311 is an RNA-binding protein, and that PAN RNA brings the CHD4 and ORF57 proteins into
312 proximity by serving as a scaffold for the biotinylation (model shown in **Fig. 5a**). In order to
313 examine the interaction of CHD4 with PAN RNA, we prepared purified RNAs (PAN RNA, MRE
314 mutant, PAN RNA deletion mutants and luciferase RNA) and proteins (CHD4, NF- κ B and
315 Luciferase) (**Fig. 5f**) and performed *in vitro* interaction assays (**depicted in Fig. 5g**). The results
316 showed that CHD4 was indeed precipitated with PAN RNA; however, MRE mutant, PAN RNA
317 deletion mutants, as well as irrelevant luciferase RNA also interacted with CHD4 protein,
318 suggesting that CHD4 RNA binding is unlikely sequence specific under our binding conditions
319 (**Fig. 5h**). However, the same RNA binding conditions with full length PAN RNA did not
320 precipitate a DNA binding protein, NF- κ B (p65) or Luciferase protein, suggesting that CHD4
321 does possess RNA-binding capacity (**Fig. 5i**). Because a previous study showed that Drosophila
322 melanogaster CHD4 homolog is capable of binding DNA and human CHD4 ATPase activity is
323 stimulated in the presence of naked DNA (76), we tested if purified CHD4 protein is able to bind
324 to double stranded (ds)DNA fragment encoding the PAN RNA sequence. Biotinylated primer
325 was used to amplify DNA fragment from the PAN RNA gene and used for biotin-pull down
326 analyses. The results showed that CHD4 was able to bind dsDNA directly (**Fig. 5j**). Importantly,
327 increasing amounts of PAN RNA (ssRNA) antagonized CHD4 dsDNA binding, which was
328 completely blocked in presence of non-biotinylated PAN RNA at 1:10 (dsDNA/RNA) molecular

329 ratio (**Fig. 5j**). The results suggested that locally transcribing long non-coding RNAs (which
330 would reach up to 3×10^5 copies/cell for PAN RNA (54)) may remove CHD4 locally from the KSHV
331 genome, as seen by reduced CHD4 on KSHV genome (**Fig. 4b**) and detachment of KSHV
332 episomes from host chromosomes during reactivation (**Fig. 4c**). These results suggest that
333 amount of long non-coding RNAs expression near the CHD4 binding sites may play a role in
334 both lytic gene induction and episome tethering.

335

336 **CHD4 is important for latency maintenance and establishment.**

337 The studies above suggest that LANA interacts with the ChAHP complex on both cellular and
338 viral chromosomes, and that the ChAHP complex may restrict KSHV enhancer activity and
339 hence KSHV lytic reactivation. Accordingly, we next examined the significance of CHD4 in the
340 KSHV transcription program. CHD4 expression in *iSLK.219* cell was knocked down with shRNA
341 and the degree of KSHV reactivation was examined after triggering K-Rta expression with
342 doxycycline. The results showed that knock-down of CHD4 enhanced KSHV replication more
343 than 8-fold over K-Rta induction alone. Conversely, functional re-introduction of CHD4 by over
344 expression of mouse *Chd4* cDNA (i.e., in order to escape from the shRNA, which targets human
345 CHD4) counteracted effects of CHD4 knock-down (**Fig. 6a**). Notably, over expression of mouse
346 *Chd4* almost completely abolished K-Rta mediated KSHV reactivation (**Fig. 6a, second bar**),
347 and inhibited the aggregation of RNAPII on the KSHV genome, which was measured by
348 immunostaining with overexpressed CHD4 and RNAPII (**Fig. 6b**). Strong silencing effects were
349 CHD4's ATPase-activity dependent, because mutations in the helicase domain, using the same
350 mutation found in patients with CHD4-associated syndrome (42, 77), was found to increase
351 RNAPII aggregation and KSHV transcription (**Fig. 6b, c**). In addition to the knock-down or over

352 expression studies, we also performed single cell transcriptomic studies with reactivated
353 iSLK.219 cells. The results clearly indicated that the presence of higher levels of CHD4 had clear
354 inhibitory effects for the triggering and/or prolonging lytic viral gene transcription burst (**Fig. 6d**).
355 Further, KSHV transcripts were extracted and sorted based on sequence counts and examined
356 for correlation with cellular gene expression at the single cell level (**Supplementary Fig. 6a, b**).
357 The results again showed a negative correlation between CHD4 expression and the amount of
358 KSHV transcripts in the cell (**Fig. 6e**), while a similar negative correlation was not observed for
359 GAPDH or similarly expressing HDAC2, a component of NuRD complex (**Supplementary Fig.**
360 **6c**).

361 Finally, the significance of CHD4 in the establishment of latency was also examined. To
362 do this, we first knocked-down CHD4 in 293T cells and infected the cells with purified KSHV
363 r.219 virus to monitor viral gene silencing. CHD4 knock-down was confirmed at the protein and
364 RNA levels (**Fig. 6f, g**). The results showed that KSHV gene expression continued to increase
365 during a 3-day period in two independent CHD4 KD cells, while KSHV gene expression did not
366 increased significantly in shScramble cells at day 3 (**Fig. 6h**). Further, KSHV lytic replication was
367 also monitored with RFP signals within the cell population, and results showed that the number
368 of RFP positive cells within the dish were higher in CHD4 knock-down 293T cells compared to
369 negative control knock-down (siC) cells at 96 hours post infection (**Fig. 6i, Supplementary Fig.**
370 **7**). Altogether, these results suggest that CHD4 functions to silence KSHV lytic genes at an early
371 stage of KSHV *de novo* infection and facilitate the entry and maintenance of latency, perhaps
372 by suppressing robust viral lncRNA expression for the viral enhancer activity.

373

374 **Discussion**

375 Recent exciting studies suggest that an RNA-binding domain in transcription factor CTCF is
376 essential for the formation of subsets of genome architecture (78, 79). The presence of distinct
377 classes of RNA-binding protein (RBP)-dependent genomic loop formation suggests the partition
378 of nascent RNAs and other RBP partners in chromatin-looping regulation at transcriptionally
379 active genomic loci. It is also known that eRNAs and RNA-binding proteins participate in
380 transcriptional factories (75, 80, 81). We show here that overexpression of CHD4 prevents
381 RNAPII aggregate formation and inhibits KSHV reactivation (**Fig. 6a,b**). Regulation of the KSHV
382 latency-lytic switch by CHD4 chromatin binding and inhibition of CHD4 DNA binding via inducible
383 transcription in cis may necessitate for KSHV to evolutionarily maintain the viral nuclear lncRNAs,
384 which are often expressed at levels 1,000x greater than the majority of KSHV protein-coding
385 RNAs during reactivation (54). Evolution of this RNA as a nuclear and non-coding species may
386 also avoid competition for protein translation and RNA export machineries, while functioning to
387 trigger robust enhancer activity for KSHV genome. Consistent with CHD4 being a strong
388 repressor, loss-of-function mutations induce enhancer activation leakage, which associates with
389 multiple developmental disorders in humans (44, 47, 82-85). We think that such CHD4 functional
390 loss may result in an increased propensity to form active enhancer-promoter interactions and
391 prolong gene transcription similar to our observations in KSHV-infected CHD4-KD 293T cells
392 (**Fig. 6h**). Consistent with CHD4 functions in enhancer access restriction, the ChAHP complex
393 is also known to compete with CTCF binding, and counteract chromatin looping at CTCF binding
394 sites. Therefore, ChAHP maintains evolutionarily conserved spatial chromatin organization by
395 preventing new CTCF binding events that emerged through short Interspersed element
396 expansions (43); this ChAHP biological role suggests that KSHV cleverly find/build a “safe
397 basecamp” with ChAHP to maintain viral episomes structure during evolution.

398 A study from Dr. Lieberman's group demonstrated that EBV episomes are tethered in the
399 neighborhood of transcriptionally silent neuronal genes (86). Our CHi-C study also found KSHV
400 episomes frequently localize at the junctions between eu- and hetero-chromatin
401 (**Supplementary Fig. 8** - junction of stripes), but more frequently localizes near centromere
402 regions than to other genomic regions. The advantage of tethering at near centromere remains
403 unknown; however, previous studies also showed that LANA dots are localized at centromeres
404 and LANA interact with centromeric protein F and kinetochore protein, Bub1(63); the two
405 proteins may play a role in recruitment of KSHV episomes to the unique genomic regions through
406 interaction with LANA.

407 The siRNA screening for epigenetic factors, which have a significant impact on KSHV
408 replication has been reported (30). The report showed that CHD4 is indeed a suppressor for
409 KSHV lytic replication. Here, we further showed that KSHV episomes are localized with ChAHP
410 on host chromatin and interact with LANA at the hydrophobic interface of LANA dimers near the
411 LANA DNA binding domain (25, 26). Suppression of KSHV lytic genes by CHD4 in *de novo*
412 infected cells also suggests that there might be active recruitment of the ChAHP complex to the
413 incoming KSHV genomes. However, the mechanism(s) that enable KSHV episomes to select
414 specific ChAHP binding sites on host chromosomes, and whether these CHD4 occupied
415 enhancers are linked to tissue-specific gene expression therefore KSHV tissue tropism have yet
416 to be characterized. At least in the three PEL cell lines examined, one of the common ChAHP-
417 LANA complex-recruitment site is IRF4 super enhancer region, which is highly active in the B-
418 cell lineage (71, 72, 87). It will be important to know if KSHV episome-bound cellular "enhancers"
419 are annexed and subjected to control by KSHV proteins in infected cells.

KSHV has been evolved to maintain a mysterious lncRNA, PAN RNA, which is expressed at a very high copy number in the presence of ORF57 protein (54), and deletion of PAN RNA or ORF57 significantly impairs the entire viral lytic gene expression program (28, 60, 88). How PAN RNA expression activates the expression of distantly localized viral open reading frames is an important question. Because PAN RNAs exceeds 10^5 copies, and CHD4 localizes at PAN RNA transcription initiation sites with LANA (**Fig. 4a**), we expect that the local PAN RNA concentration would easily result in an RNA-DNA ratio in excess of 10:1 in presence of ORF57 (57). Based on frequent genomic looping, non-coding RNA expression, and CHD4 binding (e.g., which frequently targets enhancers), we propose that the lncRNA encoding regions [Ori-RNA (T1.5), PAN RNA, K12 (T0.7)] function as inducible enhancers for expression of the KSHV ORFs, and KSHV reactivation (e.g., promoter activation) hinges on lncRNA-CHD4 interactions for the de-repression. Similar to CHD4, we previously demonstrated that PAN RNA expression also sequesters LANA from unique regions of KSHV genomes (61). Our CUT&RUN studies showed that CHD4 and LANA colocalized on both the KSHV and host genomes (**Fig. 4a**) and they could physically interact with each other (**Fig. 2d-f**); thus, we favor the idea that reactivation is triggered by detachment of LANA/ChAHP complex-loaded TR fragments from the KSHV unique region (ORFs-encoded region as well as host chromosome) by robust expression of lncRNA, whose expression is directly activated by K-Rta and enhanced by ORF57. In this proposed model, transcriptional burst by a strong viral transactivator, results in the local appearance of multiple nascent and stable-RNA copies simultaneously, in turn increasing local nucleic acid density before PAN RNA is diffused into the nuclear neighborhood. Notably, our KSHV 3D genomic structure modeling based on frequencies of ChIP-seq reads within KSHV sequences suggested that these highly inducible lncRNA encoding regions localize spatially in close proximity to TRs

443 in 3D (**Model in Fig. 6j**, Campbell et al., in preparation). The results combined with this study
444 suggest that the ChAHP-LANA complex has an architectural role for KSHV latent genomic
445 structure, and the TR region that recruits significant number of copies of both ChAHP and LANA
446 (**Fig. 4a**) is critical for episome structure and therefore suppression of lytic genes epigenetically.
447 Disruption of such a "backbone" by CHD4 KD or by robust expression of PAN RNA which binds
448 CHD4 therefore triggers "leakage" of viral lytic gene expression similarly to premature activation
449 of lineage-specific genes [(39-41) and **Fig. 6g**]. Structural studies for the ChAHP/LANA protein
450 complex with TR unit and recombinant KSHV with a LANA CHD4 binding mutant would further
451 clarify the significance of the interaction and possibly lead to small molecular drugs to target the
452 interaction.

453 In summary, we have demonstrated that the ChAHP complex is a key regulator of the
454 KSHV latency-lytic switch. With strong effects of CHD4 on KSHV replication, it will be important
455 to study how ChAHP complexes are regulated in infected cells, and also a relationship with
456 KSHV replication and KSHV-mediated disease progression in individuals who unfortunately
457 possess CHD4 mutations.

458

459 **Methods**

460 **Materials.** Dulbecco's Modified Eagle medium (DMEM), RPMI 1640 medium, fetal bovine serum
461 (FBS), phosphate buffered saline (PBS), Trypsin-EDTA solution, 100x Penicillin-streptomycin-
462 L-glutamine solution and Streptavidin-HRP conjugate were purchased from Thermo Fisher
463 Scientific (Waltham, MA USA). Puromycin and G418 solution were obtained from InvivoGen
464 (San Diego, CA, USA). Hygromycin B solution was purchased from Enzo Life Science
465 (Farmingdale, NY, USA). Anti-LANA (clone LN53), anti-Flag (clone M2) and anti-RNAPII (clone

466 CTD4H8) antibodies were purchased from Millipore-Sigma. Anti-CHD4 (D4B7), H3K27Ac
467 (D5E4) and H3K4me1 (D1A9) antibodies were purchased from Cell Signaling Technology. Anti-
468 ADNP (PA5-52286) antibody was purchased from Invitrogen. Streptavidin magnetic beads
469 (Pierce) were purchased from Thermo Fisher Scientific™. All other chemicals were purchased
470 from Millipore-Sigma (St. Louis, MO, USA) unless otherwise stated.

471

472 **Cells, transfection and reagents.** *i*SLK.219 cells were maintained in DMEM supplemented with
473 10% FBS, 1% penicillin-streptomycin-L-glutamine solution, 10 µg/ml puromycin, 400 µg/ml
474 hygromycin B, and 250 µg/ml G418. *i*SLK cells were obtained from Dr. Don Ganem (Novartis
475 Institute for Biomedical Research) and were maintained in DMEM supplemented with 10% FBS,
476 1% penicillin-streptomycin-L-glutamine solution and 10 µg/ml puromycin. BC-1 and BC-3 cell
477 lines were obtained from ATCC (Manassas, VA, USA), expanded to obtain early passage stocks,
478 and stored. The BCBL-1 cell line was also obtained from Dr. Ganem (University of California
479 San Francisco). BC-1, BC-3, and BCBL-1 cell lines were cultured in RPMI 1640 medium
480 supplemented with 15% FBS and 1% penicillin-streptomycin-L-glutamine solution. TREx BCBL-
481 1 cells, which can induce Flagx3-HAx3-K-Rta in tetracycline inducible manner, was prepared
482 before (28) were maintained in RPMI 1640 medium supplemented with 10% FBS, 1% penicillin-
483 streptomycin-L-glutamine, 250 µg/ml hygromycin B, and 100 µg/ml blasticidin. Plasmids or
484 siRNAs were transfected with Lipofectamine reagent (Thermo Fisher) or Lipofectamine
485 RNAiMax reagent (Thermo Fisher) respectively according to the manufacturer's protocol.

486 **Capture Hi-C.** KSHV Capture Hi-C (CHi-C) was performed using a robust *in situ* CHi-C protocol
487 with kitted reagents from Arima Genomics (San Diego, CA, USA) based on methods described
488 for *in situ* Hi-C (89, 90), CHi-C (91-93), and as described previously (28). Briefly, cells were

489 crosslinked with 2% formaldehyde, lysed, and the genomic DNA digested with a cocktail of 4-
490 cutter restriction endonucleases by incubation for 30 minutes at 37°C. The 5'-overhangs were
491 then filled in and labeled with biotinylated dATP (biotin-14-dATP) by incorporation with Klenow
492 fragment of DNA polymerase I (incubation for 45 minutes at 25°C). Ligation of the spatially
493 proximal blunt-ended fragments was then performed with T4 DNA ligase (incubation for 15
494 minutes at 25°C). The formaldehyde crosslinks were reversed and the proximally-ligated,
495 chimeric DNA products were purified with Agencourt AMPure XP paramagnetic beads (Beckman
496 Coulter, Brea, CA, USA). The DNA was then fragmented to an average size of 400 bp with a
497 Covaris E220 Focused-ultrasonicator (Covaris, Inc., Woburn, MA, USA) and size-selected to
498 have a fragment size distribution of 200-600 bp with AMPure XP beads. The biotin-labeled
499 ligation products were then selectively enriched by affinity capture with streptavidin magnetic
500 beads (Arima Enrichment Beads). Subsequently, sequencing libraries were prepared with the
501 Kapa HyperPrep Kit with Library Amplification Module (Roche, Basel, Switzerland) using a
502 modified protocol for on-bead end repair, dA-tailing, and ligation of Illumina TruSeq sequencing
503 adaptors.

504 The KSHV CHi-C library was then prepared from the Hi-C libraries as previously
505 described (28). Briefly, target enrichment for KSHV genomic content was performed by solution
506 hybridization with a custom-designed KSHV genomic capture probe library (xGen Lockdown
507 Probes; Integrated DNA Technologies, Inc., Coralville, IA) (28) and subsequent capture of the
508 hybridized targets with streptavidin beads (DynaBeads MyOne Streptavidin C1; Thermo Fisher)
509 according to the manufacturer's standard protocol (Integrated DNA Technologies, Inc.,
510 Coralville, IA). The KSHV genome-enriched CHi-C library DNA was eluted and PCR enrichment
511 (12 cycles) performed with high-fidelity KAPA HiFi HotStart DNA Polymerase (Kapa Biosystems,

512 Inc., Wilmington, MA). Libraries were multiplex sequenced (2 x 150bp, paired-end, ~50 million
513 mapped reads/mate pairs per sample) on an Illumina Hiseq 4000 sequencing system.

514

515 **Cleavage Under Targets and Release Using Nuclease (CUT&RUN).** CUT&RUN (70) was
516 performed essentially by following the online protocol established by Dr. Henikoff's lab with a
517 few modifications. Cells were washed with PBS and wash buffer [(20 mM HEPES-KOH pH 7.5,
518 150 mM NaCl, 0.5 mM Spermidine (Sigma, S2626) and proteinase inhibitor (Roche)]. After
519 removing the wash buffer, cells were captured on magnetic ConA beads (Polysciences, PA,
520 USA), in the presence of CaCl₂. Beads/cells complexes were washed with digitonin wash buffer
521 (0.02% digitonin, 20 mM HEPES-KOH pH 7.5, 150 mM NaCl, 0.5 mM Spermidine and 1x
522 proteinase inhibitor) 3 times, aliquoted, and incubated with specific antibodies in 250 µL volume.
523 The antibodies used in this study were: rabbit monoclonal anti-CHD4 (Cell Signaling, D4B7;
524 1:50); rat monoclonal anti-LANA (Millipore-Sigma, clone LN53; 1:50); rabbit anti-ADNP
525 polyclonal (Invitrogen, PA5-52286; 1:100); rabbit monoclonal anti-Acetylated Histone H3 lysine
526 27 (Cell Signaling, D5E4; 1:100), rabbit monoclonal anti-H3 monomethyl lysine 4 (Cell Signaling,
527 D1A9; 1:100), and rabbit monoclonal anti-H3 tri-methyl lysine 27 (Cell Signaling, C36B11;
528 1:100). After incubation, unbound antibody was removed by washing with digitonin wash buffer
529 3 times. Beads were then incubated with recombinant pAG-MNase, which was purified from
530 *E.coli* (**Supplementary Fig. 9**), in 250 µl digitonin wash buffer at 1.0 µg/mL final concentration
531 for one hour at 4°C with rotation. Unbound pAG-MNase was removed by washing with digitonin
532 wash buffer 3 times. Pre-chilled 2 mM CaCl₂ containing digitonin wash buffer (200 µL) was added
533 to beads and incubated on ice for 30 min. The pAG-MNase digestion was halted by the addition
534 of 200 µl 2× STOP solution (340 mM NaCl, 20 mM EDTA, 4 mM EGTA, 50 µg/ml RNase A, 50

535 µg/ml glycogen). The beads were incubated with shaking at 37°C for 10 min in a tube shaker at
536 500 rpm to release digested DNA fragments from the insoluble nuclear chromatin. The
537 supernatant was collected after centrifugation (16,000 x g for 5 min at 4°C) and placed on a
538 magnetic stand. DNA was extracted using the NucleoSpin kit (Takara Bio, Kusatsu, Shiga,
539 Japan). Sequencing libraries were then prepared from 3 ng of CUT&RUN DNA with the Kapa
540 HyperPrep Kit (Roche) according to the manufacturer's standard protocol. Libraries were
541 multiplex sequenced (2 x 150bp, paired-end) on an Illumina HiSeq 4000 sequencing system to
542 yield ~15 million mapped reads per sample. When necessary, *E. coli* genomic DNA read from a
543 pAG-MNase incubation were used to normalize data as described previously (70).

544

545 **Genomic data analysis.**

546 The HiC-pro 2.11.1 pipeline (94) was used to align sequences from the Hi-C experiments against
547 a combined assembly of reference genomes; the human hg19 (GRCh37) and KSHV
548 (NC_009333.1). The reads were filtered for only uniquely mapped reads pairs by identifying
549 intersection of each read-end, and the valid reads were provided by removing reads with self-
550 circle, dangling-end, error, extra dangling-end, too short, too large, duplicated, and random
551 breaks. The valid reads were stored as matrices and binned with resolution of 10000 bp. Iterative
552 Correction and Eigenvector decomposition (ICE) normalization was used to treat the data with
553 default parameters. The normalized counts were filtered to keep only the counts that mapped to
554 both the human and KSHV genome by using Python with Pandas library. The results were
555 visualized as dot plots using Matplotlib library.

556 The normalized counts were also used as input in subsequent analyses. In the analysis of KSHV
557 episome localization near centromeres, centromeres of human chromosome (hg19) were
558 downloaded from the UCSC Table Browser with a filter of 'centromere' as gap type. For each
559 chromosome, the sum of all counts was compared to both the sums of the counts in the regions
560 near the centromere at the 5' and 3' sides, both of which are 1% the size of the chromosome
561 (the values were first normalized as per 100,000 bp before the comparisons). The similarity of
562 CHi-C chimeric sequence reads among BC-1, BC-3, and BCBL-1 were performed as follows.
563 Genomic regions with normalized counts > 0 were extracted and then the intersect and union
564 regions were determined using Intervene v0.6.4 (95). The similarity percentage was calculated
565 based on the Jaccard similarity index.

566 FASTQ files for the capture Hi-C experiments were processed through the HiCUP (v0.7.4)
567 pipeline (96) using a combined human hg19 (GRCh37) and KSHV (NC_009333.1) genome.
568 Valid interaction products called by HiCUP were converted into Juicebox (97) input format (.hic
569 file), which stores the normalized and un-normalized contact matrices as a highly compressed
570 binary file, by using a series a scripts provided by HiCUP (hicup2homer) and HOMER
571 (makeTagDirectory and tagDir2hicFile) (98). Juicebox was utilized to facilitate adjustments of
572 resolution and normalization, intensity scaling, zooming, and addition of annotation tracks.

573 CUT&RUN sequence reads were aligned to the human hg38 reference genome and
574 reference KSHV genome sequence (Human herpesvirus 8 strain: GQ994935.1) with Bowtie2
575 v2.3.5.1 (99) and/or HISAT2 v2.1.0 (100). MACS2 (Model-based Analysis of ChIP-Seq)
576 v2.1.1.20160309 was used for detecting peaks (101) following the developer's manual. Peaks
577 and read alignments were visualized using the Integrated Genome Browser (IGB) (102).
578 Heatmaps and average profile plots were drawn from bed files created by MACS and bam files

579 using R package, ngsplot v2.63 (103). After subtracting the minimum value of average profile
580 as background signal, relative average profile plot was drawn. Accumulation index was
581 calculated as proportion of area under the curve.

582

583 **Single cell RNA sequencing data analysis.** Single cell data was analyzed with the Cell Ranger
584 v2.1 pipeline (10x Genomics). The pipeline included alignment to the hg38 human reference
585 genome and human herpesvirus 8 strain (GQ994935.1) reference genome, t-distributed
586 stochastic neighbor embedding (tSNE), and K-means clustering. Read count matrices obtained
587 from the pipeline were normalized using log normalization method with “Seurat” R package
588 (104). To perform correlation analysis, the expression of the KSHV genes was summarized, log
589 transformed and resulting values divided by 14 equal intervals to have more than 50 cells in
590 each interval. The median value of gene expression was calculated for the cells in each interval.
591 The median values were used to analyze and visualize the correlation of host cellular and viral
592 gene expression.

593

594 **Immunofluorescence staining analyses.** iSLK cells latently infected with BAC16-Wt were
595 seeded onto glass coverslips and transfected with pLenti-Flag-mCHD4-myc WT or pLenti-Flag-
596 mCHD4-myc mutant using Lipofectamine 2000 reagent according to the manufacturer’s
597 protocol. pLenti-Flag-mCHD4-myc was obtained from a commercial source (Origene, MD, USA).
598 Point mutations were inserted by synthesizing DNA fragments that contain intended mutations
599 and replaced at SexAI-Agel restriction sites with In-FusionHD (Takara Bio, Japan). At 24 hrs
600 after transfection, 1 µg/ml of doxycycline and 20 ng/ml of 12-O-Tetradecanoylphorbol-13-acetate

601 (TPA) were added, and cells were cultured for a further 26 hrs in the presence of doxycycline
602 and TPA. The cells were then fixed with 4% paraformaldehyde, permeabilized with 0.2% Triton
603 X-100, and labeled with anti-RNAPII mouse monoclonal antibody (Millipore-Sigma, clone
604 CTD4H8, 1:100) and anti-FLAG rabbit polyclonal antibody (Sigma, F7425, 1:100), followed by
605 Alexa 555-anti mouse IgG and Alexa 647-anti rabbit IgG (Thermo Fisher). Nuclei were
606 counterstained with 1 µg/ml of Hoechst 33342 (Thermo Fisher). The labeled cells were observed
607 with a Keyence BZ-X710 fluorescence microscope (Keyence, Osaka, Japan) with standard
608 DAPI, GFP, TRITC and Cy5 filter sets (Chroma Technologies, Bellows Falls, VT, USA).

609 **DNA-FISH combining with LANA immunostaining.** BCBL-1 cells were washed with PBS
610 twice and spotted on coverslips and fixed with 4% formaldehyde-PBS for 10 min at RT. Cells
611 were subsequently incubated with PBS with 100 mM glycine to quench residual formaldehyde.
612 Cells were treated with 0.1% Triton-X and 0.05% SDS with RNaseA for 15 min at 37°C.
613 Coverslips were washed with PBS twice, 70% ethanol once, 85% ethanol once, and 100%
614 ethanol once and dried completely. Cy5-conjugated CENPB-Cy5 PNA probe was obtained from
615 a commercial source (PNA Bio, Thousand Oaks, CA, USA) and coverslips were incubated with
616 hybridization buffer (200 nM PNA probe, 2xSSC, 20% Dextran, 1 mg/mL yeast tRNA, 60%
617 formamide) on a glass slide on a heating plate at 57°C for 10 min and then 37°C for another 30
618 min. Utilization of PNA probes avoids harsh conditions often used for a larger DNA hybridization,
619 which we found to produce unacceptable noise and not readily compatible with subsequent
620 protein staining. The coverslip was washed with warmed 0.1% Tween 20 in PBS (57°C) in 6-
621 well plates for 3 times and PBS once. Primary antibody was incubated for LANA staining in PBS
622 with 1 mg/mL yeast tRNA. After washing with PBS 3 times, secondary antibody (Alexa 488-anti
623 Rat IgG) was incubated in PBS with yeast tRNA for 1 h at 37°C. After washing three times with

624 PBS, the coverslips were mounted with antifade reagent (Thermo Fisher), and images were
625 captured with a Keyence microscope.

626 **3D Fluorescence microscopy and quantitative image analysis.** Widefield 3D fluorescence
627 imaging was performed on a Keyence BZ-X710 fluorescence microscope (Keyence, Osaka,
628 Japan) equipped with live-cell environmental chamber. Cells fluorescently labeled as previously
629 described were observed with standard DAPI, GFP, TRITC and Cy5 filter sets (Chroma
630 Technologies, Bellows Falls, VT, USA). High resolution image stacks were acquired in each
631 color channel using Keyence onboard software. Image stacks were converted to greyscale TIF
632 images that were uniformly corrected for haze reduction, deblurring and contrast enhancement.

633 Image data were subsequently exported to the Volocity® Multi-Dimensional Imaging
634 Platform (Quorum Technologies Inc., Ontario, Canada) for 3D visualization and quantitative
635 analysis. For image-based cytometry measurements, individual cells within a given field of view
636 were automatically identified and fluorescent objects and/or region of interest in the various color
637 channels were quantified and tabulated. For qualitative assessment of LANA and centromere
638 oligo probes for DNA-FISH, 3D image stacks were similarly compiled and displayed in 3D opacity
639 mode using Volocity Visualization toolset. Reconstructed 3D images were used for distance-
640 measurement analysis: briefly, fluorescent LANA dots (green) and DNA centromeres (purple) in
641 individual cell nuclei were automatically identified in Volocity Quantitation. The minimum
642 distance from each centromere to the nearest LANA dot could then be extracted from the
643 statistical measurements and displayed as histograms for subsequent analysis.

644

645 **Lentivirus production and transduction.** For CHD4 knock-down experiments, the following
646 shRNA sequences from Sigma pLKO.1 shRNA libraries were used: shRNA#1:
647 CCTTACTAGAATTGGTGTTAT; shRNA#2: GCTGACACAGTTATTATCTAT. Lentiviruses
648 generated from the CHD4-expressing lentivector, CHD4-targeting shRNAs, and non-targeting
649 scramble shRNA (Addgene, #1864) were produced in 293T cells. The vectors were co-
650 transfected with psPAX2 (Addgene, #12260) and pMD2.G (Addgene, #12259) into 293T cells
651 using polyethylenimine (PEI). Supernatants were collected 48 and 72 hrs post-transfection. Cells
652 were infected with lentiviruses in the presence of 8 µg/ml polybrene and subsequently incubated
653 for 72 hrs to allow for protein expression or knock-down. To generate CHD4 knock-down cell
654 lines, 293T cells were infected with lentivirus for 24 hrs. Cells were then cultured in selection
655 medium containing 1 µg/ml puromycin for two weeks to obtain stable CHD4 knock-down cell
656 lines.

657

658 **Preparation of purified KSHV and *de novo* infection.** iSLK.219 cells latently infected with
659 recombinant KSHV were cultured in eight to ten 150 mm culture dishes until 80% confluent. For
660 reactivation, cultures were re-fed with complete DMEM (without selection drugs) containing
661 0.3 mM sodium butyrate and 1 µg/ml doxycycline. The cells were further cultured for 5 days in
662 the presence of sodium butyrate and doxycycline. The culture supernatant was centrifuged at
663 300 x g for 10 min, and then passed through a 0.8-µm filter to remove cellular debris, and then
664 viral particles were concentrated by ultracentrifugation at 25,000 rpm for 2 hrs at 4 °C with a
665 Beckman SW28 rotor. The viral precipitates were resuspended in 500 µl of DMEM along with
666 the residual ~500 µl media in the centrifuge tube and stored at –80 °C until use. For *de novo*
667 infection, CHD4-KD 293T cells were seeded at 4 x 10⁵ cells/well in 6-well plates. After overnight

668 culture, viral stocks were added to the cultures and the infection was allowed to proceed for
669 24 hrs. Cells were monitored for GFP expression and RNA was purified using the RNeasy Mini
670 Kit (Qiagen, Venlo, Netherlands).

671

672 **Flow Cytometry.** 293T cells were transfected with 10 pmol CHD4 siRNA using Lipofectamine
673 RNAiMax reagent (Thermo Fisher) for 48 hrs. Cells were infected with r.219 virus for 96 hrs in
674 DMEM media containing 5% FBS. After that, cells were trypsinized and washed with PBS two
675 times followed by fixation with 2% PFA containing 1 mM EDTA for 10 minutes at 37 °C. Cells
676 were then washed with PBS twice and resuspended in PBS containing 1 mM EDTA. Cells were
677 passed through a 0.45-µm strainer to obtain single cells. A BD “Fortessa” cytometer was used
678 for FACS analysis, and FlowJo software (Tree Star) was used for data analysis.

679

680 **Purification of recombinant protein.** *Spodoptera frugiperda* Sf9 cells (Millipore) were
681 maintained in Ex-Cell 420 medium (Sigma), and recombinant baculoviruses were generated with
682 the Bac to bac baculovirus expression system as previously described (20, 105). Transfer
683 plasmid, pFAST-BAC1 vector was modified by inserting a Flag tag at the N-terminus, and CHD4,
684 ORF57, p65, and Luciferase cDNAs were cloned into the Cpol (*RsrII*) site. The cDNA of ADNP,
685 which also include C-terminal His tag was synthesized and cloned into *Bam*HI and *Pst*I restriction
686 enzyme sites by Gene assembly (NEB). Recombinant baculovirus bacmid DNA was transfected
687 into Sf9 cells by using polyethylenimine (Sigma), and recombinant viruses were subsequently
688 amplified twice. Expression of recombinant proteins was confirmed by immunoblotting with anti-
689 Flag monoclonal antibody (Sigma). Large-scale cultures of Sf9 cells (100 ml) were infected with

690 recombinant baculovirus at a multiplicity of infection (MOI) of 0.1 to 1.0, and cells were harvested
691 48 hrs after infection. Recombinant proteins were purified as described previously (106). The
692 purity and amount of protein were measured by SDS-PAGE and Coomassie blue staining, using
693 bovine serum albumin (BSA) as a standard.

694

695 ***In vitro* interaction assays.** Baculoviruses expressing Flag-CHD4, His-ADNP, or Flag-LANA
696 were co-infected in SF9 cells and purified by Flag tag capture in the presence of 500 mM NaCl
697 and 10% glycerol. Purified complex was re-suspended in the binding buffer (20 mM HEPES [pH
698 7.9], 150 mM NaCl, 1 mM EDTA, 4 mM MgCl₂, 1 mM dithiothreitol, 0.02% NP-40, 10% glycerol
699 supplemented with 1 mg/ml BSA, and 1× protease inhibitor cocktail) and the antibody was
700 incubated at 1:100 dilution for 1 hrs at 4°C to form an immunocomplex. The immunocomplex
701 was captured with 10 µL of protein A/G magnetic beads mixture. Beads were washed three
702 times with binding buffer and subjected to SDS-PAGE after eluting proteins in sample buffer.
703 The interaction was probed by immunoblotting with anti-CHD4, anti-ADNP, or anti-LANA
704 antibody.

705 For RNA or DNA pull-down, a final concentration of 100 nM of each biotinylated RNA
706 fragment (e.g. 1.3 µg for full length PAN RNA transcribed *in vitro* or 2.6 µg of dsDNA generated
707 by PCR with 5'-biotinylated primer) and purified proteins (100 nM in final) was incubated in RNA-
708 binding buffer (50 mM HEPES [pH 7.9], 150 mM KCl, 5% glycerol, 0.02% NP-40, 100 µg/mL
709 yeast tRNA, 2 mM MgCl₂) supplemented with RNase inhibitor in 40 µL reaction for 1 hrs at 4°C.
710 Biotinylated RNA or dsDNA was captured with streptavidin conjugated magnetic beads, washed
711 with binding buffer 3 times, and proteins were eluted in sample buffer. Precipitated proteins were

712 visualized by immunoblotting with either anti-Flag antibody (Sigma) or specific antibody as
713 indicated in figure legends.

714

715 **Construction of mini-Turbo KSHV BAC16.** Recombinant KSHV was prepared by following a
716 protocol for En passant mutagenesis with a two-step markerless red recombination technique
717 (107). Briefly, the codon optimized mini-TurboID coding sequence (65), which also encodes the
718 3x Flag tag was first cloned into a pBS SK vector (Thermo Fisher, Waltham, MA USA). The
719 pEPkan-S plasmid was used as a source of the kanamycin cassette, which includes the I-SceI
720 restriction enzyme site at the 5'-end of the kanamycin coding region (107). The kanamycin
721 cassette was amplified with primer pairs with homology arms and cloned into the mini-TurboID
722 coding region at a unique restriction enzyme site. The resulting plasmid was used as a template
723 for another round of PCR to prepare a transfer DNA fragment for markerless recombination with
724 BAC16 (108). Recombinant BAC16 clones with insertion and also a deletion of the kanamycin
725 cassette in the BAC16 genome were confirmed by colony PCR with appropriate primer pairs.
726 Recombination junctions and adjacent genomic regions were amplified by PCR and the resulting
727 PCR products were directly sequenced with the same primers to confirm in-frame insertion of
728 the mini-TurboID cassette into the BAC16 DNA for mini-TurboID-ORF57 and -LANA. Insertion
729 of PAN RNA MRE mutations was performed by using primer pairs that encode the intended
730 mutations. Primer pairs were used to amplify the kanamycin cassette and recombination,
731 deletion of kanamycin cassette, confirmation of mutations was performed as described above.
732 The resulting recombinant BAC16 was confirmed by restriction enzyme digestions (*Hind*III and
733 *Bg*II) to determine if there were any large DNA deletions. Two independent BAC16 clones were
734 generated for each mini-TurboID tagged recombinant KSHV virus as biological replicates and

735 one of the clones was used for protein ID. Entire BAC16 DNAs were subsequently sequenced
736 by NGS on an Illumina MiSeq System.

737 **Quantification of viral copy number.** Two hundred microliters of cell culture supernatant were
738 treated with DNase I (12 µg/ml) for 15 min at room temperature to degrade unencapsidated
739 DNA. This reaction was stopped by the addition of EDTA to 5 mM followed by heating at 70°C
740 for 15 min. Viral genomic DNA was purified using the QIAamp DNA Mini Kit according to the
741 manufacturer's protocol and eluted in 100 µl of buffer AE. Four microliters of the eluate were
742 used for real-time qPCR to determine viral copy number, as described previously (105).

743

744 **Real-time RT-PCR.** Total RNA was isolated using the Quick-RNA miniprep kit (Zymo Research,
745 Irvine, CA, USA). First-strand cDNA was synthesized using the High Capacity cDNA Reverse
746 Transcription Kit (Thermo Fisher, Waltham, MA USA). Gene expression was analyzed by
747 realtime qPCR using specific primers for KSHV ORFs designed by Fakhari and Dittmer (109).
748 We used 18S ribosomal RNA or GAPDH as an internal standard to normalize viral gene
749 expression.

750

751 **Western blotting.** Cells were lysed in IP lysis buffer (25 mM Tris-HCl pH 7.4, 150 mM NaCl, 1%
752 NP-40, 1 mM EDTA, 5% glycerol) containing protease inhibitors (Roche, Basel, Switzerland).
753 Total cell lysates (25 µg) were boiled in SDS-PAGE loading buffer and subjected to SDS-PAGE
754 and subsequently transferred to a polyvinylidene fluoride membrane (Millipore-Sigma, St. Louis,
755 MO, USA) using a semidry transfer apparatus (Bio-Rad, Hercules, CA, USA). The streptavidin-
756 HRP conjugate was used at 1:3000 dilution. Final dilution of the primary antibody was 1:3,000

757 for anti-Flag mouse antibody, 1:1,000 for anti-LANA rat antibody, anti-CHD4 rabbit, and anti-
758 ADNP rabbit antibodies. Washing membranes and secondary antibody incubations were
759 performed as described previously (105).

760

761 **Affinity purification of biotinylated proteins.** KSHV LANA-mTID cells were incubated with
762 100 µM D-biotin for 60 mins at 37°C. To stop the reaction, cells were incubated at 4°C for 60
763 mins. Cells were washed with cold PBS three times followed by lysis with SUMO lysis buffer
764 (Tris-Cl PH 6.8, 1% SDS and 10% glycerol). Lysates were immediately boiled for 10 min, and
765 protein was quantified by Bradford assay (Bio-Rad). The biotinylation signal was confirmed by
766 western blotting using Strep-HRP.

767 Affinity purification was performed with streptavidin-coated magnetic beads (Thermo-Fisher).
768 Briefly, 150 µl magnetic beads/sample were pre-washed with RIPA lysis buffer (150 mM NaCl,
769 5 mM EDTA (pH 8), 50 mM Tris (pH 8), 1% NP-40, 0.5% sodium deoxycholate, 0.1% SDS) 3
770 times. A total of 3 mg of whole cell lysate was incubated with pre-washed streptavidin beads
771 after diluting with RIPA buffer for 10 times, at room temperature for 1h with rotation. The beads
772 were collected using a magnetic stand and washed three times with wash buffer according to
773 the manufacturer's protocol. Finally, beads were resuspended in 200 µl of wash buffer and sent
774 to UC Davis Proteomics core for on bead digestion and LC-MS/MS analysis.

775

776 **MS sample preparation.** Protein samples on magnetic beads were washed four times with 200
777 µl of 50 mM ammonium bicarbonate (AMBIC) with a twenty-minute shake time at 4°C in between
778 each wash. Roughly 2.5 µg of trypsin was added to the beads and AMBIC and the samples were

779 digested overnight at 800 rpm shake speed. After overnight digestion, the supernatant was
780 removed, and the beads were washed once with enough 50 mM AMBIC to cover them. After 20
781 minutes at a gentle shake the wash was removed and combined with the initial supernatant. The
782 peptide extracts were reduced in volume by vacuum centrifugation and a small portion of the
783 extract was used for fluorometric peptide quantification (Thermo Scientific Pierce). One
784 microgram of sample based on the fluorometric peptide assay was loaded for each LC-MS
785 analysis.

786 Digested peptides were analyzed by LC-MS/MS on a Thermo Scientific Q Exactive
787 Orbitrap Mass spectrometer in conjunction with Proxeon Easy-nLC II HPLC (Thermo Scientific)
788 and Proxeon nanospray source. The digested peptides were loaded on a 100 micron x 25 mm
789 Magic C18 100Å 5U reverse phase trap where they were desalted online before being separated
790 using a 75-micron x 150 mm Magic C18 200Å 3U reverse-phase column. Peptides were eluted
791 using a 60-minute gradient with a flow rate of 300 µl/min. An MS survey scan was obtained for
792 the m/z range 300-1600, MS/MS spectra were acquired using a top 15 method, where the top
793 15 ions in the MS spectra were subjected to HCD (High Energy Collisional Dissociation). An
794 isolation mass window of 2.0 m/z was used for the precursor ion selection, and normalized
795 collision energy of 27% was used for fragmentation. A fifteen second duration was used for the
796 dynamic exclusion.

797

798 **MS/MS analysis.** Tandem mass spectra were extracted and charge state deconvoluted by
799 Proteome Discoverer (Thermo Scientific). All MS/MS samples were analyzed using X! Tandem
800 (The GPM, thegpm.org; version X! Tandem Alanine (2017.2.1.4)). X! Tandem was set up to
801 search the Human and Kaposi's Sarcoma Herpes virus database (149182 entries) assuming the

802 digestion enzyme trypsin. X! Tandem was searched with a fragment ion mass tolerance of 20
803 PPM and a parent ion tolerance of 20 PPM. Carbamidomethyl of cysteine and selenocysteine
804 was specified in X! Tandem as a fixed modification. Glu->pyro-Glu of the N-terminus, ammonia-
805 loss of the N-terminus, gln->pyro-Glu of the N-terminus, deamination of asparagine and
806 glutamine, oxidation of methionine and tryptophan and dioxidation of methionine and tryptophan
807 were specified in X! Tandem as variable modifications.

808 Scaffold (version Scaffold_4.8.4, Proteome Software Inc., Portland, OR) was used to
809 validate MS/MS-based peptide and protein identifications. Peptide identifications were accepted
810 if they could be established at greater than 98.0% probability by the Scaffold Local FDR
811 algorithm. Peptide identifications were also required to exceed specific database search engine
812 thresholds. Protein identifications were accepted if they could be established at greater than
813 5.0% probability to achieve an FDR less than 5.0% and contained at least 2 identified peptides.
814 Protein probabilities were assigned by the Protein Prophet algorithm (110). Proteins that
815 contained similar peptides and could not be differentiated based on MS/MS analysis alone were
816 grouped to satisfy the principles of parsimony. Proteins sharing significant peptide evidence
817 were grouped into clusters.

818

819 **Pathway analysis.** The proteins identified to be interacting with ORF57 were used for gene
820 ontology analysis. The top gene ontology processes were enriched by the Metascape web-
821 based platform, and the Metascape software was used for gene ontology analysis (111).

822

823 **Statistical analysis.** Results are shown as mean \pm SD from at least three independent
824 experiments. Data were analyzed using unpaired Student's t test, or ANOVA followed by Tukey's
825 HSD test. A value of p<0.05 was considered statistically significant.

826

827 **Code availability.** All custom codes used to analyze data and generate figures are available
828 upon request.

829

830 **Data availability.** Data can be accessed via the Source Data files and Supplementary tables.
831 The genomic data discussed in this publication have been deposited in NCBI's GEO Database
832 under unified Super Series GSE163695 with subseries GSE163098 for CUT&RUN and
833 GSE163694 for CHi-C.

834

835 **Acknowledgement.** This research was supported by public health grants from the National
836 Cancer Institute (CA225266, CA232845), the National Institute of Dental and Craniofacial
837 (DE025985), and the National Institute of Allergy and Infectious Disease (AI147207) to Y.I. The
838 Genomics Shared Resource is supported by the UC Davis Comprehensive Cancer Center
839 Support Grant (CCSG) awarded by the National Cancer Institute (NCI P30CA093373).

840

841 **Author Contributions.**

842 A.K., Y.L., M.C., and Y.I. designed and performed experiments, analyzed data and prepared
843 figures. Y.Y., C.C., R.R.D., K.N., and A.M. ran genomic pipelines, performed statistical analyses,

844 and visualized genomic data sets. M.S. prepared enzyme digested protein samples and performed
845 proteomics data analyses. R.R.D. and C.G.T. prepared sequencing libraries and performed initial
846 bioinformatics analyses. K.I.N and R.R.D. prepared single cell transcriptomics libraries, and A.M.
847 wrote custom codes and analyzed single-cell sequence data sets. A.K., Y.L., K.W., C.I., and Y.I.
848 prepared BAC stable cell lines, and performed molecular and biochemical studies. YI generated
849 recombinant BACs. F.C. and K.I.N. prepared slides and performed imaging analyses. V.M., M.S.,
850 and Z.M.Z. contributed key reagents. A.K, Y.L., Y.Y., C.C., M.S., F.C., R.R.D., C.G.T., K.N., K.I.N.,
851 V.M., Z.M.Z. and Y.I. analyzed corresponding data sets. Y.I. wrote the manuscript and all authors
852 edited the manuscript.

853

854 **Competing financial interests.**

855 The authors have declared that no conflicts of interest exist.

856

857 **Materials & Correspondence.**

858 Correspondence and request for materials should be addressed to M.C. (e-mail:
859 mcampbell@ucdavis.edu) or Y.I. (email: yizumiya@ucdavis.edu).

860

861 **Figure legends**

862 **Fig. 1 KSHV episome-tethering sites in KSHV positive cell lines. (a) Schematic workflow**

863 **for Capture-HiC (CHi-C). (b) KSHV episome-docking sites on host cell chromosomes.**

864 CHi-C chimeric DNA ligation products composed of sequences derived from the KSHV and

865 human genomes were mapped in three naturally-infected PEL cells. For BCBL-1 cells, three

866 biological replicates were performed with nearly identical results (similarity 0.95). M,

867 mitochondrial chromosome. ICE-corrected profiles depicting sums of filtered read counts binned

868 at 10 kb resolution are shown. **(c) Selected chromosome 1 in zoomed view.** Chromosome 1

869 dot plots were depicted, which displays enrichment of sequence reads near the centromere. Red

870 arrows indicate the position of the centromere. Extended panels for all other individual

871 chromosome for three cell lines are presented in Supplementary Fig. 1a-c. **(d) KSHV episomes**

872 **preferentially localize near the centromere.** KSHV episome contacts were calculated in

873 BCBL-1 cells for sequence reads in 1% (length of the respective chromosome) of the 5'-and 3'-

874 centromere and compared with the average of the total chromosome read count. **(e) LANA**

875 **protein locates near the centromere.** DNA-FISH was used to visualize the location of the

876 centromere (red) and KSHV episomes were indirectly visualized by staining LANA dots (Green)

877 in BCBL-1 cells. The centromere and LANA were probed using a Cenp probe and anti-LANA

878 antibody respectively with IFA. The two signals were frequently co-localized, and 3D view and

879 their image analyses are presented in Supplementary Fig. 2. **(f) Jaccard statistics and Venn**

880 **diagram.** Venn diagram shows percent similarity of KSHV episome-tethering positions among

881 BC-1, BC-3 and BCBL-1 cells.

882

883 **Fig. 2 LANA interacts with the ChAHP complex. (a) A schematic diagram of preparation**
884 **of recombinant KSHV infected *i*SLK cells.** A mini-TurboID (mTID) was fused to the N-terminus
885 of the LANA open reading frame to generate KSHV LANA-mTID. KSHV LANA-mTID was
886 transfected into *i*SLK cells followed by production of viral particles by stimulating cells with
887 doxycycline (1 µg/ml) and sodium butyrate (3 mM) for 5 days. Virus was used to infect *i*SLK cells
888 and cells were selected with hygromycin (1 mg/ml) to obtain an *i*SLK-LANA mTID stable cell
889 line. **(b) Experimental design for preparing samples for protein ID.** *i*SLK-LANA mTID cells
890 were left un-incubated (-) or incubated (+) with D-Biotin (500 µM) for 1 hr. Unincubated (-) cells
891 were used as control samples. Each protein ID was performed in three biological replicates. **(c)**
892 **Volcano plot depicting proteins in close proximity to LANA.** The volcano plot represents
893 proteins identified in close proximity to LANA. Proteins with an abundance Log2 FC of greater
894 than or equal to 1 and p-value less than 0.05 were selected and are shown by blue box. T-test
895 was used for calculating the p-value. Purple color; ChAHP components. Red color; previously
896 identified proteins as LANA interacting proteins. **(d) LANA interacts with CHD4 and ADNP *in***
897 ***vitro*.** LANA, CHD4 and ADNP complex, which consists of Flag-LANA (gold arrow), Flag-CHD4
898 (blue arrow), and His-ADNP (green arrow) was prepared by co-infected three recombinant
899 baculoviruses, and the protein complex was isolated in the presence of 500 mM NaCl and 10%
900 glycerol with affinity purification. The authenticity of respective protein band was confirmed by
901 immunoblotting with specific antibodies. Coomassie staining is shown. An equimolar amount
902 (100 nM) of the three proteins were incubated in binding buffer and immunoprecipitated with the
903 specific antibodies of one another. Ten percent of the reaction before immunoprecipitation was
904 shown as controls. W.B: Western Blotting, Co-IP: Co-immunoprecipitation. **(e) CHD4**
905 **interaction site on LANA.** Purified GST-tagged LANA deletions, Flag-tagged luciferase and

906 Flag-tagged CHD4 were prepared from recombinant baculovirus infected Sf9 cells. An equal
907 amount (1 µg) of each LANA deletion protein was incubated with full length Flag-tagged
908 luciferase (1 µg) or Flag-tagged CHD4 (1 µg) in binding buffer and interaction was probed with
909 anti-Flag antibody. LANA deletion proteins used for this GST-pull down assay are presented in
910 Supplementary Fig. 4. **(f) LANA co-localizes with CHD4 in BCBL-1.** CHD4 and LANA were
911 probed with anti-CHD4 rabbit monoclonal antibody and anti-LANA rat monoclonal antibody,
912 respectively. Images were taken with Keyence fluorescence microscopy. Scale bar (20 µm) is
913 shown.

914

915 **Fig. 3 Association of ChAHP complex binding with KSHV episome-tethering sites. (a)**
916 **CUT&RUN analysis for LANA, ADNP, CHD4 and H3K27Ac.** The indicated antibodies were
917 used for CUT&RUN in BCBL-1 cells. CUT&RUN peaks were visualized with Integrative
918 Genomics Viewer (IGV) and a snapshot of one of the major binding sites (IRF4 super enhancer
919 region) is shown. The number on the left-hand side denotes the height of the peak (e.g., read
920 depth) and the number along the top denotes the positions on chromosome 6. **(b) Heatmaps**
921 **for co-occupancies of LANA with ADNP, CHD4 and H3K27Ac on chromosomes.** Heatmap
922 (middle) and average profile (bottom) showing correlation of LANA enrichment (by color intensity
923 and region) with ADNP, CHD4, and H3K27Ac occupancies. Average profile plot summarizing
924 the heatmap (bottom). The lighter green shade represents the standard error (SEM) on the
925 average profile plot. Color keys are shown on the each heatmap (top). **(c) Heatmaps for**
926 **correlation of CHi-C with CUT&RUN signals.** The association between CHi-C chimeric reads
927 and LANA, CHD4, ADNP and H3K4me1 CUT&RUN peaks were depicted as heatmap and
928 average profile plot. **(d) Accumulation index around CHD4 binding sites.** The accumulation

929 of CHD4 is displayed as a proportion of area under the curve of the relative average profile.
930 Association between distance from CHD4 summit peak and relative chimeric sequence counts
931 is shown as a bar chart.

932

933 **Fig. 4 LANA, CHD4 and ADNP colocalize on the KSHV genome. (a) CUT&RUN analysis.**
934 The indicated antibodies were used for CUT&RUN in BCBL-1 cells and sequence reads were
935 mapped to the KSHV genome. An IGV snapshot and KSHV genome map are shown. The
936 number on the left-hand side denotes the height of the peak (e.g., read depth), the number along
937 the top denotes the position on KSHV genome in kilobase (kb) and the number on the right-hand
938 side indicated by arrow denote the height of the peak on terminal repeat region (TR). Selected
939 region is zoomed in to show Ori-RNA and PAN RNA region. Primer used in Fig. 4b is also shown
940 with red arrows and number show the exact location of the amplified region by the primers. **(b)**
941 **Regulation of CHD4 on the KSHV episome during reactivation.** TREx-BCBL-1 cells were
942 reactivated with doxycycline (1 µg/ml) and sodium butyrate (3 mM) for 24 hrs. CUT&RUN was
943 performed on un-reactivated (latency) and reactivated cells for CHD4. CHD4 binding on the PAN
944 RNA promoter region (**red arrow in Fig. 4a, right panel**) was calculated relative to the input
945 sample (n=3, two biological replicates are shown). **(c) Detachment of KSHV episomes by**
946 **reactivation.** BCBL-1 cells were reactivated with doxycycline (1 µg/ml) and TPA (20 nM) for 24
947 hrs. Chimeric sequence reads for un-reactivated (latency) and reactivated cells were mapped to
948 the host chromosomes and visualized by Juicebox. Relative KSHV episome tethering during
949 reactivation for the selected region on chromosome 1 was calculated by subtracting relative
950 chimeric sequence reads in latency from relative chimeric sequence reads during reactivation.
951 Blue and red dots indicate decreased and increased chimeric sequence reads respectively.

952

953 **Fig. 5 CHD4 is both an RNA and DNA binding protein. (a) A schematic diagram of**
954 **recombinant KSHVs.** Mini-TurboID is fused to the N-terminus of ORF57 open reading frame
955 and the ORF57 binding site (MRE) of PAN RNA was mutated as shown. **(b) Immunoblotting.**
956 Recombinant KSHV infected iSLK cells (TID-57 PAN-Wt and -MRE) were either untreated or
957 induced for reactivation with doxycycline (1 µg/ml) and TPA (20 nM) for 24 hrs. Blots were probed
958 with either anti-Flag antibody (for mini-TurboID-ORF57) or Streptavidin-HRP (for biotinylated
959 proteins). **(c) Venn diagram.** The Venn diagram indicates the number of identified proteins with
960 a P value less than 0.05. Each protein ID was performed in three biological replicates. **(d) PAN**
961 **RNA-mediated interacting proteins with ORF57.** The proteins found enriched in PAN RNA-
962 WT samples are shown. The entire list of proteins and peptide counts are presented in
963 Supplementary Table 2. **(e) siRNA screening with KSHV reactivation as readout.**
964 Recombinant KSHV reactivation, which encodes RFP under control of the PAN RNA promoter,
965 was used to screen the effects of KSHV reactivation. RFP signal intensity was measured with
966 Image J, and the GFP signal was used as internal controls. Three randomly selected fields in
967 the middle of each well were quantified and the average intensity was plotted. **(f) Recombinant**
968 **proteins and synthesized PAN RNAs.** Recombinant Flag-tagged proteins were expressed with
969 baculovirus and purified with Flag-agarose beads. Coomassie staining of Flag-CHD4, Flag-NF-
970 kB (p65), and Flag-luciferase used for pull-down studies are shown. **(g) Schematic for *in vitro***
971 **interaction assay performed in Fig. 5 (h-j).** **(h) CHD4 binds RNAs in a sequence-**
972 **independent manner.** RNA pull-down was performed with the indicated biotinylated PAN RNA
973 deletions, mutation (MRE), and irrelevant RNA (luciferase mRNA), and interaction was probed
974 by immunoblotting with anti-Flag antibody. Beads alone (No RNA) was used for background

control. **(i)** RNA pull down was performed with indicated biotinylated RNAs, and p65 and Luciferase (Luc) were visualized by using anti-Flag antibody. **(j) PAN RNA competes with CHD4 DNA binding.** Pull-down analyses with biotinylated ssRNA or dsDNA was performed. CHD4 (100 nM) was incubated with biotinylated RNA (100 nM) or biotinylated dsDNA (100 nM) in 40 μ L binding buffer. Increasing amounts of non-biotinylated PAN RNA at 1:1, 1:10, and 1:20 (dsDNA vs. ssRNA) were also incubated, and precipitated CHD4 protein in the pull-down was probed with anti-Flag antibody. Flow-through and 10% of the input reaction before pull-down were used as control.

983

Fig. 6 CHD4 is important for latency maintenance and establishment. (a) CHD4 overexpression, knockdown and complementation. The *i*SLK.219 cell line was transfected with empty vector (Vec) or mouse CHD4 cDNA or human CHD4 shRNA, or CHD4 shRNA and mouse CHD4 cDNA for 48 hrs followed by KSHV reactivation with doxycycline (1 μ g/ml) for 5 days. Encapsidated KSHV genomes in the culture supernatants were measured by qPCR to assess effects of CHD4 overexpression or knockdown on KSHV reactivation. **(b) CHD4 ATPase activity is important for prevention of nuclear aggregate formation.** *i*SLK cells latently infected with BAC16-Wt was transfected with Flag-tagged mouse wild type CHD4, or an ATPase domain mutant was transfected and stained with anti-Flag. Transcriptional factory formation was assessed by staining RNAII. The percentage of aggregate formation in Flag-positive cells was measured and plotted. Three biological replicates were performed, and 50 cells were counted in each of the three biological replicates. **(c) CHD4 ATPase activity is important for inhibiting viral gene expression during reactivation.** *i*SLK.219 cells were transduced with an equal amount of CHD4 wild type (wt) and CHD4 mutant (mt) lentivirus for 2 days. Cells were

998 reactivated with doxycycline (1 µg/ml) for 2 days and ORF50 and ORF57 gene expression was
999 quantified by RT-qPCR. Untreated cells were used for calculating the relative expression of
1000 ORF50 and ORF57. GAPDH was used as a negative control. *p<0.05, ***p<0.001 (comparing
1001 with CHD4 Wt). **(d-e) Single cell sequencing.** *i*SLK.219 cells were reactivated by induction of
1002 K-Rta expression from doxycycline inducible promoter for 24 hrs. Single-cell sequencing was
1003 performed with the 10x Genomics platform. A cell suspension was prepared followed by cell
1004 partitioning and 3' cDNA synthesis on the Chromium Controller and dual-index library
1005 preparation with 10x Genomics kitted reagents. **(d) tSNE.** tSNE was applied to separate cell
1006 clusters and KSHV gene (**d, left panel**) and CHD4 (**d, right panel**) expressing cells were marked.
1007 **(e) Negative correlation between CHD4 and viral gene expression.** Cells were divided into
1008 groups based on the amount of KSHV transcripts. A table and distribution of cell numbers and
1009 amount of KSHV transcripts are shown in Supplementary Fig. 6a-b. Intervals used to separate
1010 cell groups are also listed in Supplementary Fig. 6b. A correlation was established based on
1011 CHD4 expression in different groups of KSHV transcripts. **(f-h) CHD4 knockdown and KSHV**
1012 **lytic gene expression during *de novo* infection.** 293T cells were transduced with scramble
1013 shRNA (shScrm) or shCHD4 and stably selected with antibiotic. Immunoblot (**f**) and RT-qPCR
1014 (**g**) analysis of CHD4 in the 293T stable cell lines are shown. 293T stable cells were infected
1015 with rKSHV.219 for 24 hrs and total RNA was harvested at the indicated time points. **(h)** K-Rta
1016 and PAN RNA, was measured by RT-qPCR and normalized to GAPDH. *p<0.05, **p<0.01
1017 (comparing with shScrm). **(i) Flow cytometry.** 293T cells were transfected with control siRNA
1018 (siC) or CHD4 siRNA (siCHD4) for 48 hrs followed by infection with rKSHV.219 virus for 96 hrs.
1019 Flow cytometry analysis was performed to calculate the number of GFP- and RFP-positive cells
1020 in siC and siCHD4 knockdown cells. **(j) KSHV latency model with ChAHP.** KSHV episomes

1021 tether at epigenetically active regions with the ChAHP complex, and TR-loaded LANA/ChAHP
1022 prevents robust viral lncRNA expression. The action of robust lncRNA expression in lytic KSHV
1023 infection functions as an enhancer for viral ORFs that are physically neighboring with lncRNA
1024 genomic regions. Stimulation of K-Rta, in part by decreased CHD4 expression, triggers robust
1025 PAN RNA expression in the presence of ORF57, which competes with CHD4 DNA binding to
1026 enhance KSHV reactivation and detach KSHV episomes from CHD4-enriched host chromosome
1027 regions.

1028

1029

1030 **Reference**

- 1031 1. **Chang Y, Cesarman E, Pessin MS, Lee F, Culpepper J, Knowles DM, Moore PS.** 1994. Identification of
1032 herpesvirus-like DNA sequences in AIDS-associated Kaposi's sarcoma. *Science* **266**:1865-1869.
- 1033 2. **Ganem D.** 2010. KSHV and the pathogenesis of Kaposi sarcoma: listening to human biology and medicine.
1034 *J Clin Invest* **120**:939-949.
- 1035 3. **Mesri EA, Cesarman E, Boshoff C.** 2010. Kaposi's sarcoma and its associated herpesvirus. *Nat Rev Cancer*
1036 **10**:707-719.
- 1037 4. **Schulz TF.** 2006. The pleiotropic effects of Kaposi's sarcoma herpesvirus. *J Pathol* **208**:187-198.
- 1038 5. **Wong EL, Damania B.** 2005. Linking KSHV to human cancer. *Curr Oncol Rep* **7**:349-356.
- 1039 6. **Cesarman E, Moore PS, Rao PH, Inghirami G, Knowles DM, Chang Y.** 1995. In vitro establishment and
1040 characterization of two acquired immunodeficiency syndrome-related lymphoma cell lines (BC-1 and BC-
1041 2) containing Kaposi's sarcoma-associated herpesvirus-like (KSHV) DNA sequences. *Blood* **86**:2708-2714.
- 1042 7. **Cesarman E, Knowles DM.** 1999. The role of Kaposi's sarcoma-associated herpesvirus (KSHV/HHV-8) in
1043 lymphoproliferative diseases. *Semin Cancer Biol* **9**:165-174.
- 1044 8. **Kedes DH, Lagunoff M, Renne R, Ganem D.** 1997. Identification of the gene encoding the major latency-
1045 associated nuclear antigen of the Kaposi's sarcoma-associated herpesvirus. *J Clin Invest* **100**:2606-2610.
- 1046 9. **Nakamura H, Lu M, Gwack Y, Souvlis J, Zeichner SL, Jung JU.** 2003. Global changes in Kaposi's sarcoma-
1047 associated virus gene expression patterns following expression of a tetracycline-inducible Rta
1048 transactivator. *J Virol* **77**:4205-4220.
- 1049 10. **Lu M, Suen J, Frias C, Pfeiffer R, Tsai MH, Chuang E, Zeichner SL.** 2004. Dissection of the Kaposi's sarcoma-
1050 associated herpesvirus gene expression program by using the viral DNA replication inhibitor cidofovir. *J
1051 Virol* **78**:13637-13652.
- 1052 11. **Ellison TJ, Izumiya Y, Izumiya C, Luciw PA, Kung HJ.** 2009. A comprehensive analysis of recruitment and
1053 transactivation potential of K-Rta and K-bZIP during reactivation of Kaposi's sarcoma-associated
1054 herpesvirus. *Virology* **387**:76-88.
- 1055 12. **Ballestas ME, Kaye KM.** 2011. The latency-associated nuclear antigen, a multifunctional protein central
1056 to Kaposi's sarcoma-associated herpesvirus latency. *Future Microbiol* **6**:1399-1413.
- 1057 13. **Stedman W, Deng Z, Lu F, Lieberman PM.** 2004. ORC, MCM, and histone hyperacetylation at the Kaposi's
1058 sarcoma-associated herpesvirus latent replication origin. *J Virol* **78**:12566-12575.
- 1059 14. **Verma SC, Choudhuri T, Kaul R, Robertson ES.** 2006. Latency-associated nuclear antigen (LANA) of
1060 Kaposi's sarcoma-associated herpesvirus interacts with origin recognition complexes at the LANA binding
1061 sequence within the terminal repeats. *J Virol* **80**:2243-2256.
- 1062 15. **Hu J, Garber AC, Renne R.** 2002. The latency-associated nuclear antigen of Kaposi's sarcoma-associated
1063 herpesvirus supports latent DNA replication in dividing cells. *J Virol* **76**:11677-11687.
- 1064 16. **Barbera AJ, Chodaparambil JV, Kelley-Clarke B, Joukov V, Walter JC, Luger K, Kaye KM.** 2006. The
1065 nucleosomal surface as a docking station for Kaposi's sarcoma herpesvirus LANA. *Science* **311**:856-861.
- 1066 17. **Pilot T, Tramier M, Coppey M, Nicolas JC, Marechal V.** 2001. Close but distinct regions of human
1067 herpesvirus 8 latency-associated nuclear antigen 1 are responsible for nuclear targeting and binding to
1068 human mitotic chromosomes. *J Virol* **75**:3948-3959.
- 1069 18. **Ottinger M, Christalla T, Nathan K, Brinkmann MM, Viejo-Borbolla A, Schulz TF.** 2006. Kaposi's sarcoma-
1070 associated herpesvirus LANA-1 interacts with the short variant of BRD4 and releases cells from a BRD4-
1071 and BRD2/RING3-induced G1 cell cycle arrest. *J Virol* **80**:10772-10786.
- 1072 19. **Matsumura S, Persson LM, Wong L, Wilson AC.** 2010. The latency-associated nuclear antigen interacts
1073 with MeCP2 and nucleosomes through separate domains. *J Virol* **84**:2318-2330.

- 1074 20. **Kim KY, Huerta SB, Izumiya C, Wang DH, Martinez A, Shevchenko B, Kung HJ, Campbell M, Izumiya Y.**
1075 2013. Kaposi's sarcoma-associated herpesvirus (KSHV) latency-associated nuclear antigen regulates the
1076 KSHV epigenome by association with the histone demethylase KDM3A. *J Virol* **87**:6782-6793.
- 1077 21. **Wang N, Wu R, Tang D, Kang R.** 2021. The BET family in immunity and disease. *Signal Transduct Target*
1078 *Ther* **6**:23.
- 1079 22. **You J, Srinivasan V, Denis GV, Harrington WJ, Jr., Ballesteras ME, Kaye KM, Howley PM.** 2006. Kaposi's
1080 sarcoma-associated herpesvirus latency-associated nuclear antigen interacts with bromodomain protein
1081 Brd4 on host mitotic chromosomes. *J Virol* **80**:8909-8919.
- 1082 23. **Hu J, Yang Y, Turner PC, Jain V, McIntyre LM, Renne R.** 2014. LANA binds to multiple active viral and
1083 cellular promoters and associates with the H3K4methyltransferase hSET1 complex. *PLoS Pathog*
1084 **10**:e1004240.
- 1085 24. **Lagunoff M, Ganem D.** 1997. The structure and coding organization of the genomic termini of Kaposi's
1086 sarcoma-associated herpesvirus. *Virology* **236**:147-154.
- 1087 25. **Domsic JF, Chen HS, Lu F, Marmorstein R, Lieberman PM.** 2013. Molecular basis for oligomeric-DNA
1088 binding and episome maintenance by KSHV LANA. *PLoS Pathog* **9**:e1003672.
- 1089 26. **Correia B, Cerqueira SA, Beauchemin C, Pires de Miranda M, Li S, Ponnusamy R, Rodrigues L, Schneider**
1090 **TR, Carrondo MA, Kaye KM, Simas JP, McVey CE.** 2013. Crystal structure of the gamma-2 herpesvirus
1091 LANA DNA binding domain identifies charged surface residues which impact viral latency. *PLoS Pathog*
1092 **9**:e1003673.
- 1093 27. **Kim J, Dean A.** 2021. Enhancers navigate the three-dimensional genome to direct cell fate decisions. *Curr*
1094 *Opin Struct Biol* **71**:101-109.
- 1095 28. **Campbell M, Watanabe T, Nakano K, Davis RR, Lyu Y, Tepper CG, Durbin-Johnson B, Fujimuro M, Izumiya**
1096 **Y.** 2018. KSHV episomes reveal dynamic chromatin loop formation with domain-specific gene regulation.
1097 *Nat Commun* **9**:49.
- 1098 29. **Chen CP, Lyu Y, Chuang F, Nakano K, Izumiya C, Jin D, Campbell M, Izumiya Y.** 2017. Kaposi's Sarcoma-
1099 Associated Herpesvirus Hijacks RNA Polymerase II To Create a Viral Transcriptional Factory. *J Virol* **91**.
- 1100 30. **Naik NG, Nguyen TH, Roberts L, Fischer LT, Glickman K, Golas G, Papp B, Toth Z.** 2020. Epigenetic factor
1101 siRNA screen during primary KSHV infection identifies novel host restriction factors for the lytic cycle of
1102 KSHV. *PLoS Pathog* **16**:e1008268.
- 1103 31. **Strahan RC, McDowell-Sargent M, Uppal T, Purushothaman P, Verma SC.** 2017. KSHV encoded ORF59
1104 modulates histone arginine methylation of the viral genome to promote viral reactivation. *PLoS Pathog*
1105 **13**:e1006482.
- 1106 32. **Rossetto CC, Pari G.** 2012. KSHV PAN RNA associates with demethylases UTX and JMJD3 to activate lytic
1107 replication through a physical interaction with the virus genome. *PLoS Pathog* **8**:e1002680.
- 1108 33. **Gunther T, Frohlich J, Herrde C, Ohno S, Burkhardt L, Adler H, Grundhoff A.** 2019. A comparative
1109 epigenome analysis of gammaherpesviruses suggests cis-acting sequence features as critical mediators of
1110 rapid polycomb recruitment. *PLoS Pathog* **15**:e1007838.
- 1111 34. **Toth Z, Maglinte DT, Lee SH, Lee HR, Wong LY, Brulois KF, Lee S, Buckley JD, Laird PW, Marquez VE, Jung**
1112 **JU.** 2010. Epigenetic analysis of KSHV latent and lytic genomes. *PLoS Pathog* **6**:e1001013.
- 1113 35. **Gunther T, Grundhoff A.** 2010. The epigenetic landscape of latent Kaposi sarcoma-associated herpesvirus
1114 genomes. *PLoS Pathog* **6**:e1000935.
- 1115 36. **Clarkson CT, Deeks EA, Samarista R, Mamayusupova H, Zhurkin VB, Teif VB.** 2019. CTCF-dependent
1116 chromatin boundaries formed by asymmetric nucleosome arrays with decreased linker length. *Nucleic*
1117 *Acids Res* **47**:11181-11196.
- 1118 37. **Barisic D, Stadler MB, Iurlaro M, Schubeler D.** 2019. Mammalian ISWI and SWI/SNF selectively mediate
1119 binding of distinct transcription factors. *Nature* **569**:136-140.
- 1120 38. **Goodman JV, Yamada T, Yang Y, Kong L, Wu DY, Zhao G, Gabel HW, Bonni A.** 2020. The chromatin
1121 remodeling enzyme Chd4 regulates genome architecture in the mouse brain. *Nat Commun* **11**:3419.

- 1122 39. **Ostapcuk V, Mohn F, Carl SH, Basters A, Hess D, Iesmantavicius V, Lampersberger L, Flemr M, Pandey A, Thoma NH, Betschinger J, Buhler M.** 2018. Activity-dependent neuroprotective protein recruits HP1 and CHD4 to control lineage-specifying genes. *Nature* **557**:739-743.
- 1123 40. **Sun X, Yu W, Li L, Sun Y.** 2020. ADNP Controls Gene Expression Through Local Chromatin Architecture by Association With BRG1 and CHD4. *Front Cell Dev Biol* **8**:553.
- 1124 41. **Arends T, Dege C, Bortnick A, Danhorn T, Knapp JR, Jia H, Harmacek L, Fleenor CJ, Straign D, Walton K, Leach SM, Feeney AJ, Murre C, O'Connor BP, Hagman JR.** 2019. CHD4 is essential for transcriptional repression and lineage progression in B lymphopoiesis. *Proc Natl Acad Sci U S A* **116**:10927-10936.
- 1125 42. **Farnung L, Ochmann M, Cramer P.** 2020. Nucleosome-CHD4 chromatin remodeler structure maps human disease mutations. *Elife* **9**.
- 1126 43. **Kaaij LJ, Mohn F, van der Weide RH, de Wit E, Buhler M.** 2019. The ChAHP Complex Counteracts Chromatin Looping at CTCF Sites that Emerged from SINE Expansions in Mouse. *Cell* **178**:1437-1451 e1414.
- 1127 44. **Zhao H, Han Z, Liu X, Gu J, Tang F, Wei G, Jin Y.** 2017. The chromatin remodeler Chd4 maintains embryonic stem cell identity by controlling pluripotency- and differentiation-associated genes. *J Biol Chem* **292**:8507-8519.
- 1128 45. **Wang HC, Chou CL, Yang CC, Huang WL, Hsu YC, Luo CW, Chen TJ, Li CF, Pan MR.** 2019. Over-Expression of CHD4 Is an Independent Biomarker of Poor Prognosis in Patients with Rectal Cancers Receiving Concurrent Chemoradiotherapy. *Int J Mol Sci* **20**.
- 1129 46. **Xia L, Huang W, Bellani M, Seidman MM, Wu K, Fan D, Nie Y, Cai Y, Zhang YW, Yu LR, Li H, Zahnow CA, Xie W, Chiu Yen RW, Rassool FV, Baylin SB.** 2017. CHD4 Has Oncogenic Functions in Initiating and Maintaining Epigenetic Suppression of Multiple Tumor Suppressor Genes. *Cancer Cell* **31**:653-668 e657.
- 1130 47. **Kovac K, Sauer A, Macinkovic I, Awe S, Finkernagel F, Hoffmeister H, Fuchs A, Muller R, Rathke C, Langst G, Brehm A.** 2018. Tumour-associated missense mutations in the dMi-2 ATPase alters nucleosome remodelling properties in a mutation-specific manner. *Nat Commun* **9**:2112.
- 1131 48. **Weiss K, Terhal PA, Cohen L, Brucolieri M, Irving M, Martinez AF, Rosenfeld JA, Machol K, Yang Y, Liu P, Walkiewicz M, Beuten J, Gomez-Ospina N, Haude K, Fong CT, Enns GM, Bernstein JA, Fan J, Gotway G, Ghorbani M, Study DDD, van Gassen K, Monroe GR, van Haaften G, Basel-Vanagaite L, Yang XJ, Campeau PM, Muenke M.** 2016. De Novo Mutations in CHD4, an ATP-Dependent Chromatin Remodeler Gene, Cause an Intellectual Disability Syndrome with Distinctive Dysmorphisms. *Am J Hum Genet* **99**:934-941.
- 1132 49. **Sartorelli V, Lauberth SM.** 2020. Enhancer RNAs are an important regulatory layer of the epigenome. *Nat Struct Mol Biol* **27**:521-528.
- 1133 50. **Bose DA, Donahue G, Reinberg D, Shiekhattar R, Bonasio R, Berger SL.** 2017. RNA Binding to CBP Stimulates Histone Acetylation and Transcription. *Cell* **168**:135-149 e122.
- 1134 51. **Hah N, Murakami S, Nagari A, Danko CG, Kraus WL.** 2013. Enhancer transcripts mark active estrogen receptor binding sites. *Genome Res* **23**:1210-1223.
- 1135 52. **Rahnamoun H, Lee J, Sun Z, Lu H, Ramsey KM, Komives EA, Lauberth SM.** 2018. RNAs interact with BRD4 to promote enhanced chromatin engagement and transcription activation. *Nat Struct Mol Biol* **25**:687-697.
- 1136 53. **Morf J, Basu S, Amaral PP.** 2020. RNA, Genome Output and Input. *Front Genet* **11**:589413.
- 1137 54. **Song MJ, Brown HJ, Wu TT, Sun R.** 2001. Transcription activation of polyadenylated nuclear rna by rta in human herpesvirus 8/Kaposi's sarcoma-associated herpesvirus. *J Virol* **75**:3129-3140.
- 1138 55. **Sun R, Lin SF, Gradoville L, Miller G.** 1996. Polyadenylated nuclear RNA encoded by Kaposi sarcoma-associated herpesvirus. *Proc Natl Acad Sci U S A* **93**:11883-11888.
- 1139 56. **Conrad NK, Steitz JA.** 2005. A Kaposi's sarcoma virus RNA element that increases the nuclear abundance of intronless transcripts. *EMBO J* **24**:1831-1841.
- 1140 57. **Massimelli MJ, Kang JG, Majerciak V, Le SY, Liewehr DJ, Steinberg SM, Zheng ZM.** 2011. Stability of a long noncoding viral RNA depends on a 9-nt core element at the RNA 5' end to interact with viral ORF57 and cellular PABPC1. *Int J Biol Sci* **7**:1145-1160.

- 1170 58. **Mitton-Fry RM, DeGregorio SJ, Wang J, Steitz TA, Steitz JA.** 2010. Poly(A) tail recognition by a viral RNA
1171 element through assembly of a triple helix. *Science* **330**:1244-1247.
- 1172 59. **Massimelli MJ, Majerciak V, Kruhlak M, Zheng ZM.** 2013. Interplay between polyadenylate-binding
1173 protein 1 and Kaposi's sarcoma-associated herpesvirus ORF57 in accumulation of polyadenylated nuclear
1174 RNA, a viral long noncoding RNA. *J Virol* **87**:243-256.
- 1175 60. **Rossetto CC, Tarrant-Elorza M, Verma S, Purushothaman P, Pari GS.** 2013. Regulation of viral and cellular
1176 gene expression by Kaposi's sarcoma-associated herpesvirus polyadenylated nuclear RNA. *J Virol* **87**:5540-
1177 5553.
- 1178 61. **Campbell M, Kim KY, Chang PC, Huerta S, Shevchenko B, Wang DH, Izumiya C, Kung HJ, Izumiya Y.** 2014.
1179 A lytic viral long noncoding RNA modulates the function of a latent protein. *J Virol* **88**:1843-1848.
- 1180 62. **Withers JB, Li ES, Vallery TK, Yario TA, Steitz JA.** 2018. Two herpesviral noncoding PAN RNAs are
1181 functionally homologous but do not associate with common chromatin loci. *PLoS Pathog* **14**:e1007389.
- 1182 63. **Xiao B, Verma SC, Cai Q, Kaul R, Lu J, Saha A, Robertson ES.** 2010. Bub1 and CENP-F can contribute to
1183 Kaposi's sarcoma-associated herpesvirus genome persistence by targeting LANA to kinetochores. *J Virol*
1184 **84**:9718-9732.
- 1185 64. **Branon TC, Bosch JA, Sanchez AD, Udeshi ND, Svinkina T, Carr SA, Feldman JL, Perrimon N, Ting AY.**
1186 2018. Efficient proximity labeling in living cells and organisms with TurboID. *Nat Biotechnol* **36**:880-887.
- 1187 65. **Kumar A, Salemi M, Bhullar R, Guevara-Plunkett S, Lyu Y, Wang KH, Izumiya C, Campbell M, Nakajima
1188 KI, Izumiya Y.** 2021. Proximity Biotin Labeling Reveals KSHV Interferon Regulatory Factor Networks. *J Virol*
1189 doi:10.1128/JVI.02049-20.
- 1190 66. **Hellert J, Weidner-Glunde M, Krausze J, Richter U, Adler H, Fedorov R, Pietrek M, Ruckert J, Ritter C,
1191 Schulz TF, Luhrs T.** 2013. A structural basis for BRD2/4-mediated host chromatin interaction and oligomer
1192 assembly of Kaposi sarcoma-associated herpesvirus and murine gammaherpesvirus LANA proteins. *PLoS
1193 Pathog* **9**:e1003640.
- 1194 67. **Verma SC, Cai Q, Kreider E, Lu J, Robertson ES.** 2013. Comprehensive analysis of LANA interacting proteins
1195 essential for viral genome tethering and persistence. *PLoS One* **8**:e74662.
- 1196 68. **Si H, Verma SC, Lampson MA, Cai Q, Robertson ES.** 2008. Kaposi's sarcoma-associated herpesvirus-
1197 encoded LANA can interact with the nuclear mitotic apparatus protein to regulate genome maintenance
1198 and segregation. *J Virol* **82**:6734-6746.
- 1199 69. **Lim C, Lee D, Seo T, Choi C, Choe J.** 2003. Latency-associated nuclear antigen of Kaposi's sarcoma-
1200 associated herpesvirus functionally interacts with heterochromatin protein 1. *J Biol Chem* **278**:7397-7405.
- 1201 70. **Skene PJ, Henikoff S.** 2017. An efficient targeted nuclease strategy for high-resolution mapping of DNA
1202 binding sites. *Elife* **6**.
- 1203 71. **Manzano M, Gunther T, Ju H, Nicholas J, Bartom ET, Grundhoff A, Gottwein E.** 2020. Kaposi's Sarcoma-
1204 Associated Herpesvirus Drives a Super-Enhancer-Mediated Survival Gene Expression Program in Primary
1205 Effusion Lymphoma. *mBio* **11**.
- 1206 72. **Wang C, Zhang L, Ke L, Ding W, Jiang S, Li D, Narita Y, Hou I, Liang J, Li S, Xiao H, Gottwein E, Kaye KM,
1207 Teng M, Zhao B.** 2020. Primary effusion lymphoma enhancer connectome links super-enhancers to
1208 dependency factors. *Nat Commun* **11**:6318.
- 1209 73. **Garber AC, Shu MA, Hu J, Renne R.** 2001. DNA binding and modulation of gene expression by the latency-
1210 associated nuclear antigen of Kaposi's sarcoma-associated herpesvirus. *J Virol* **75**:7882-7892.
- 1211 74. **Purushothaman P, Thakker S, Verma SC.** 2015. Transcriptome analysis of Kaposi's sarcoma-associated
1212 herpesvirus during de novo primary infection of human B and endothelial cells. *J Virol* **89**:3093-3111.
- 1213 75. **Arnold PR, Wells AD, Li XC.** 2019. Diversity and Emerging Roles of Enhancer RNA in Regulation of Gene
1214 Expression and Cell Fate. *Front Cell Dev Biol* **7**:377.
- 1215 76. **Morra R, Lee BM, Shaw H, Tuma R, Mancini EJ.** 2012. Concerted action of the PHD, chromo and motor
1216 domains regulates the human chromatin remodelling ATPase CHD4. *FEBS Lett* **586**:2513-2521.

- 1217 77. Weiss K, Lazar HP, Kurolap A, Martinez AF, Paperna T, Cohen L, Smeland MF, Whalen S, Heide S, Keren
1218 B, Terhal P, Irving M, Takaku M, Roberts JD, Petrovich RM, Schrier Vergano SA, Kenney A, Hove H,
1219 DeChene E, Quinonez SC, Colin E, Ziegler A, Rumble M, Jain M, Monteil D, Roeder ER, Nugent K, van
1220 Haeringen A, Gambello M, Santani A, Medne L, Krock B, Skraban CM, Zackai EH, Dubbs HA, Smol T,
1221 Ghoumid J, Parker MJ, Wright M, Turnpenny P, Clayton-Smith J, Metcalfe K, Kurumizaka H, Gelb BD,
1222 Baris Feldman H, Campeau PM, Muenke M, Wade PA, Lachlan K. 2020. The CHD4-related syndrome: a
1223 comprehensive investigation of the clinical spectrum, genotype-phenotype correlations, and molecular
1224 basis. *Genet Med* **22**:389-397.
- 1225 78. Hansen AS, Hsieh TS, Cattoglio C, Pustova I, Saldana-Meyer R, Reinberg D, Darzacq X, Tjian R. 2019.
1226 Distinct Classes of Chromatin Loops Revealed by Deletion of an RNA-Binding Region in CTCF. *Mol Cell*
1227 **76**:395-411 e313.
- 1228 79. Saldana-Meyer R, Rodriguez-Hernaez J, Escobar T, Nishana M, Jacome-Lopez K, Nora EP, Bruneau BG,
1229 Tsirigos A, Furlan-Magaril M, Skok J, Reinberg D. 2019. RNA Interactions Are Essential for CTCF-Mediated
1230 Genome Organization. *Mol Cell* **76**:412-422 e415.
- 1231 80. Nair SJ, Yang L, Meluzzi D, Oh S, Yang F, Friedman MJ, Wang S, Suter T, Alshareedah I, Gamliel A, Ma Q,
1232 Zhang J, Hu Y, Tan Y, Ohgi KA, Jayani RS, Banerjee PR, Aggarwal AK, Rosenfeld MG. 2019. Phase
1233 separation of ligand-activated enhancers licenses cooperative chromosomal enhancer assembly. *Nat Struct Mol Biol*
1234 **26**:193-203.
- 1235 81. Isoda T, Moore AJ, He Z, Chandra V, Aida M, Denholtz M, Piet van Hamburg J, Fisch KM, Chang AN, Fahl
1236 SP, Wiest DL, Murre C. 2017. Non-coding Transcription Instructs Chromatin Folding and
1237 Compartmentalization to Dictate Enhancer-Promoter Communication and T Cell Fate. *Cell* **171**:103-119
1238 e118.
- 1239 82. Coe BP, Stessman HAF, Sulovari A, Geisheker MR, Bakken TE, Lake AM, Dougherty JD, Lein ES,
1240 Hormozdiari F, Bernier RA, Eichler EE. 2019. Neurodevelopmental disease genes implicated by de novo
1241 mutation and copy number variation morbidity. *Nat Genet* **51**:106-116.
- 1242 83. Sifrim A, Hitz MP, Wilsdon A, Breckpot J, Turki SH, Thienpont B, McRae J, Fitzgerald TW, Singh T,
1243 Swaminathan GJ, Prigmore E, Rajan D, Abdul-Khalil H, Banka S, Bauer UM, Bentham J, Berger F,
1244 Bhattacharya S, Bu'Lock F, Canham N, Colgiu IG, Cosgrove C, Cox H, Daehnert I, Daly A, Danesh J, Fryer
1245 A, Gewillig M, Hobson E, Hoff K, Homfray T, Study I, Kahlert AK, Ketley A, Kramer HH, Lachlan K, Lampe
1246 AK, Louw JJ, Manickara AK, Manase D, McCarthy KP, Metcalfe K, Moore C, Newbury-Ecob R, Omer SO,
1247 Ouwehand WH, Park SM, Parker MJ, Pickardt T, Pollard MO, et al. 2016. Distinct genetic architectures
1248 for syndromic and nonsyndromic congenital heart defects identified by exome sequencing. *Nat Genet*
1249 **48**:1060-1065.
- 1250 84. Zhao S, Choi M, Overton JD, Bellone S, Roque DM, Cocco E, Guzzo F, English DP, Varughese J, Gasparrini
1251 S, Bortolomai I, Buza N, Hui P, Abu-Khalaf M, Ravaggi A, Bignotti E, Bandiera E, Romani C, Todeschini P,
1252 Tassi R, Zanotti L, Carrara L, Pecorelli S, Silasi DA, Ratner E, Azodi M, Schwartz PE, Rutherford TJ, Stiegler
1253 AL, Mane S, Boggon TJ, Schlessinger J, Lifton RP, Santin AD. 2013. Landscape of somatic single-nucleotide
1254 and copy-number mutations in uterine serous carcinoma. *Proc Natl Acad Sci U S A* **110**:2916-2921.
- 1255 85. Le Gallo M, O'Hara AJ, Rudd ML, Urick ME, Hansen NF, O'Neil NJ, Price JC, Zhang S, England BM, Godwin
1256 AK, Sgroi DC, Program NIHSSCCS, Hieter P, Mullikin JC, Merino MJ, Bell DW. 2012. Exome sequencing of
1257 serous endometrial tumors identifies recurrent somatic mutations in chromatin-remodeling and ubiquitin
1258 ligase complex genes. *Nat Genet* **44**:1310-1315.
- 1259 86. Kim KD, Tanizawa H, De Leo A, Vladimirova O, Kossenkov A, Lu F, Showe LC, Noma KI, Lieberman PM.
1260 2020. Epigenetic specifications of host chromosome docking sites for latent Epstein-Barr virus. *Nat Commun*
1261 **11**:877.
- 1262 87. Carbone A, Gloghini A, Cozzi MR, Capello D, Steffan A, Monini P, De Marco L, Gaidano G. 2000.
1263 Expression of MUM1/IRF4 selectively clusters with primary effusion lymphoma among lymphomatous
1264 effusions: implications for disease histogenesis and pathogenesis. *Br J Haematol* **111**:247-257.

- 1265 88. **Majerciak V, Pripuzova N, McCoy JP, Gao SJ, Zheng ZM.** 2007. Targeted disruption of Kaposi's sarcoma-
1266 associated herpesvirus ORF57 in the viral genome is detrimental for the expression of ORF59, K8alpha,
1267 and K8.1 and the production of infectious virus. *J Virol* **81**:1062-1071.
- 1268 89. **Rao SS, Huntley MH, Durand NC, Stamenova EK, Bochkov ID, Robinson JT, Sanborn AL, Machol I, Omer
1269 AD, Lander ES, Aiden EL.** 2014. A 3D map of the human genome at kilobase resolution reveals principles
1270 of chromatin looping. *Cell* **159**:1665-1680.
- 1271 90. **Belaghzal H, Dekker J, Gibcus JH.** 2017. Hi-C 2.0: An optimized Hi-C procedure for high-resolution genome-
1272 wide mapping of chromosome conformation. *Methods* **123**:56-65.
- 1273 91. **Schmitt AD, Hu M, Ren B.** 2016. Genome-wide mapping and analysis of chromosome architecture. *Nature
1274 Reviews Molecular Cell Biology* **17**:743-755.
- 1275 92. **Schoenfelder S, Javierre B-M, Furlan-Magaril M, Wingett SW, Fraser P.** 2018. Promoter Capture Hi-C:
1276 High-resolution, Genome-wide Profiling of Promoter Interactions. *Journal of Visualized Experiments : JoVE*
1277 doi:10.3791/57320.
- 1278 93. **Jung I, Schmitt A, Diao Y, Lee AJ, Liu T, Yang D, Tan C, Eom J, Chan M, Chee S, Chiang Z, Kim C, Masliah
1279 E, Barr CL, Li B, Kuan S, Kim D, Ren B.** 2019. A compendium of promoter-centered long-range chromatin
1280 interactions in the human genome. *Nat Genet* **51**:1442-1449.
- 1281 94. **Servant N, Varoquaux N, Lajoie BR, Viara E, Chen CJ, Vert JP, Heard E, Dekker J, Barillot E.** 2015. HiC-Pro:
1282 an optimized and flexible pipeline for Hi-C data processing. *Genome Biol* **16**:259.
- 1283 95. **Khan A, Mathelier A.** 2017. Intervene: a tool for intersection and visualization of multiple gene or genomic
1284 region sets. *BMC Bioinformatics* **18**:287.
- 1285 96. **Wingett S, Ewels P, Furlan-Magaril M, Nagano T, Schoenfelder S, Fraser P, Andrews S.** 2015. HiCUP:
1286 pipeline for mapping and processing Hi-C data. *F1000Res* **4**:1310.
- 1287 97. **Durand NC, Robinson JT, Shamim MS, Machol I, Mesirov JP, Lander ES, Aiden EL.** 2016. Juicebox Provides
1288 a Visualization System for Hi-C Contact Maps with Unlimited Zoom. *Cell Syst* **3**:99-101.
- 1289 98. **Heinz S, Benner C, Spann N, Bertolino E, Lin YC, Laslo P, Cheng JX, Murre C, Singh H, Glass CK.** 2010.
1290 Simple combinations of lineage-determining transcription factors prime cis-regulatory elements required
1291 for macrophage and B cell identities. *Mol Cell* **38**:576-589.
- 1292 99. **Langmead B, Salzberg SL.** 2012. Fast gapped-read alignment with Bowtie 2. *Nat Methods* **9**:357-359.
- 1293 100. **Kim D, Paggi JM, Park C, Bennett C, Salzberg SL.** 2019. Graph-based genome alignment and genotyping
1294 with HISAT2 and HISAT-genotype. *Nat Biotechnol* **37**:907-915.
- 1295 101. **Zhang Y, Liu T, Meyer CA, Eeckhoute J, Johnson DS, Bernstein BE, Nusbaum C, Myers RM, Brown M, Li
1296 W, Liu XS.** 2008. Model-based analysis of ChIP-Seq (MACS). *Genome Biol* **9**:R137.
- 1297 102. **Freese NH, Norris DC, Loraine AE.** 2016. Integrated genome browser: visual analytics platform for
1298 genomics. *Bioinformatics* **32**:2089-2095.
- 1299 103. **Shen L, Shao N, Liu X, Nestler E.** 2014. ngs.plot: Quick mining and visualization of next-generation
1300 sequencing data by integrating genomic databases. *BMC Genomics* **15**:284.
- 1301 104. **Stuart T, Butler A, Hoffman P, Hafemeister C, Papalexi E, Mauck WM, 3rd, Hao Y, Stoeckius M, Smibert
1302 P, Satija R.** 2019. Comprehensive Integration of Single-Cell Data. *Cell* **177**:1888-1902 e1821.
- 1303 105. **Izumiya Y, Izumiya C, Hsia D, Ellison TJ, Luciw PA, Kung HJ.** 2009. NF-kappaB serves as a cellular sensor
1304 of Kaposi's sarcoma-associated herpesvirus latency and negatively regulates K-Rta by antagonizing the
1305 RBP-Jkappa coactivator. *J Virol* **83**:4435-4446.
- 1306 106. **Izumiya Y, Ellison TJ, Yeh ET, Jung JU, Luciw PA, Kung HJ.** 2005. Kaposi's sarcoma-associated herpesvirus
1307 K-bZIP represses gene transcription via SUMO modification. *J Virol* **79**:9912-9925.
- 1308 107. **Tischer BK, Smith GA, Osterrieder N.** 2010. En passant mutagenesis: a two step markerless red
1309 recombination system. *Methods Mol Biol* **634**:421-430.
- 1310 108. **Brulois KF, Chang H, Lee AS, Ensser A, Wong LY, Toth Z, Lee SH, Lee HR, Myoung J, Ganem D, Oh TK, Kim
1311 JF, Gao SJ, Jung JU.** 2012. Construction and manipulation of a new Kaposi's sarcoma-associated
1312 herpesvirus bacterial artificial chromosome clone. *J Virol* **86**:9708-9720.

- 1313 109. **Fakhari FD, Dittmer DP.** 2002. Charting latency transcripts in Kaposi's sarcoma-associated herpesvirus by
1314 whole-genome real-time quantitative PCR. *J Virol* **76**:6213-6223.
- 1315 110. **Nesvizhskii AI, Keller A, Kolker E, Aebersold R.** 2003. A statistical model for identifying proteins by tandem
1316 mass spectrometry. *Anal Chem* **75**:4646-4658.
- 1317 111. **Zhou Y, Zhou B, Pache L, Chang M, Khodabakhshi AH, Tanaseichuk O, Benner C, Chanda SK.** 2019.
1318 Metascape provides a biologist-oriented resource for the analysis of systems-level datasets. *Nat Commun*
1319 **10**:1523.

1320

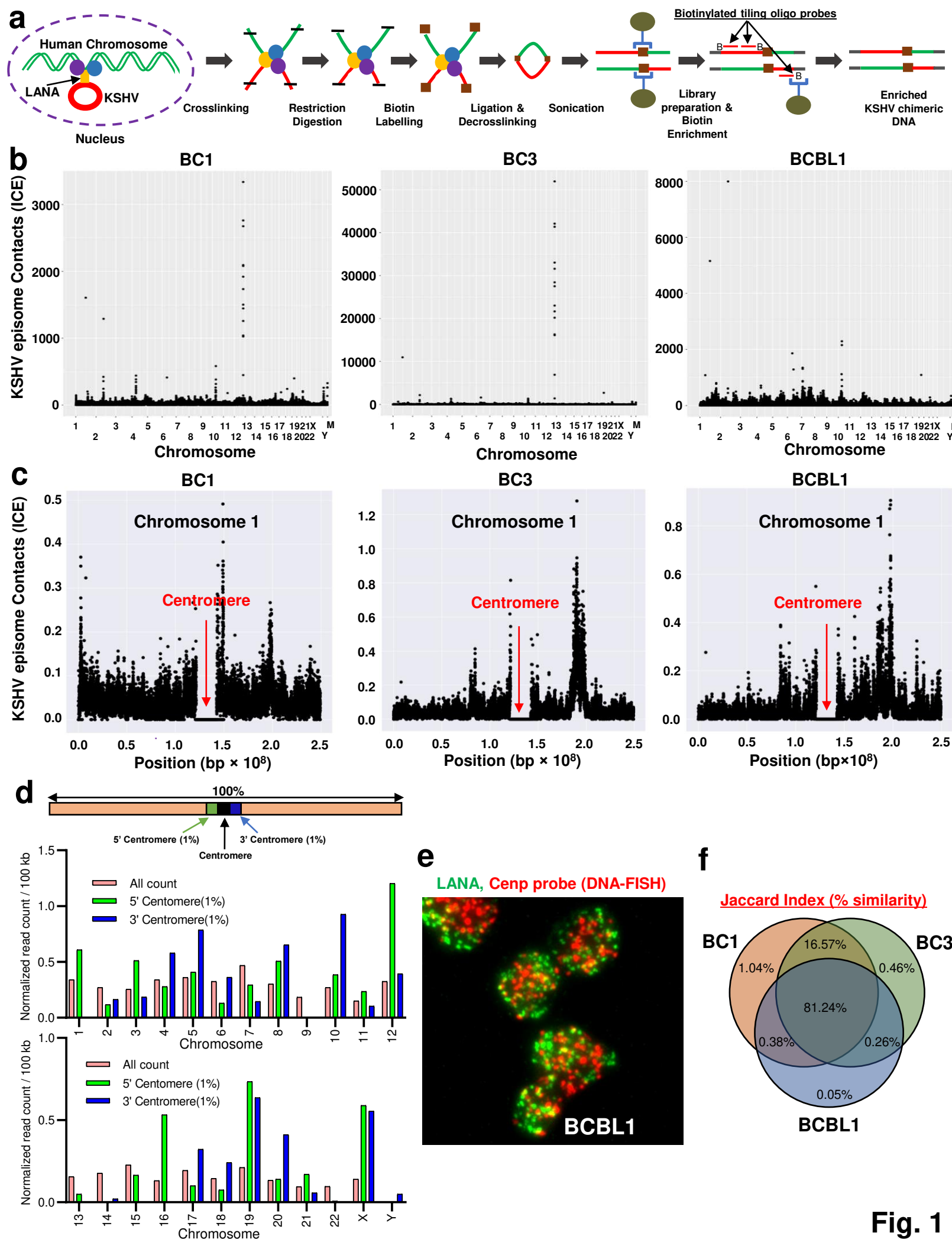
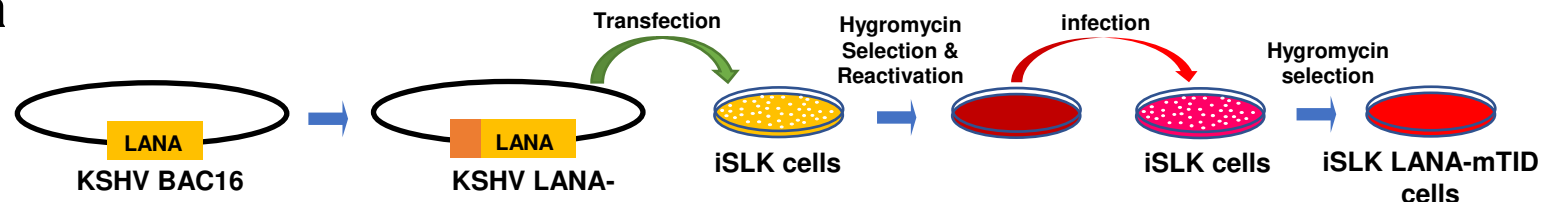
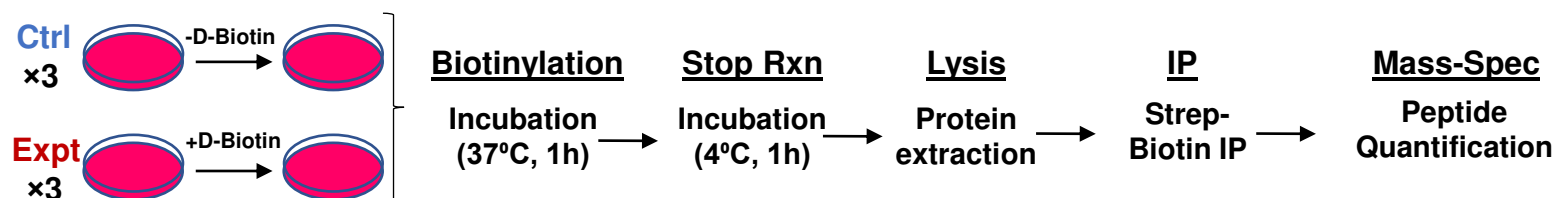
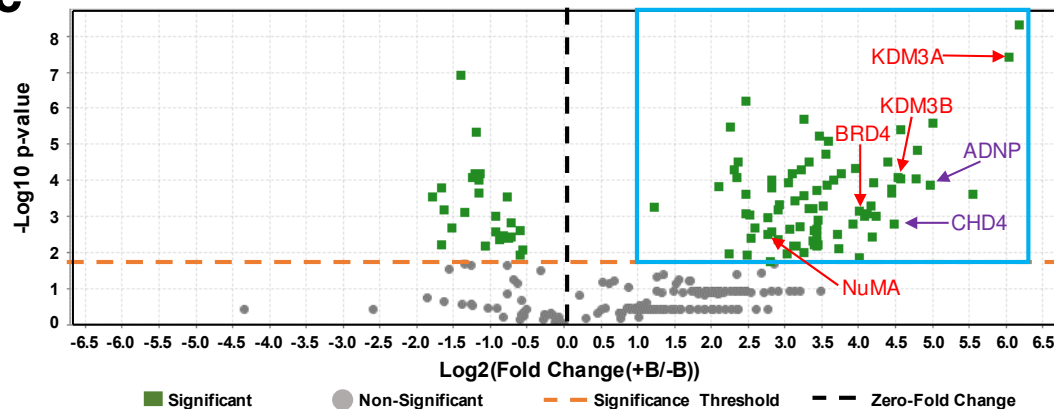
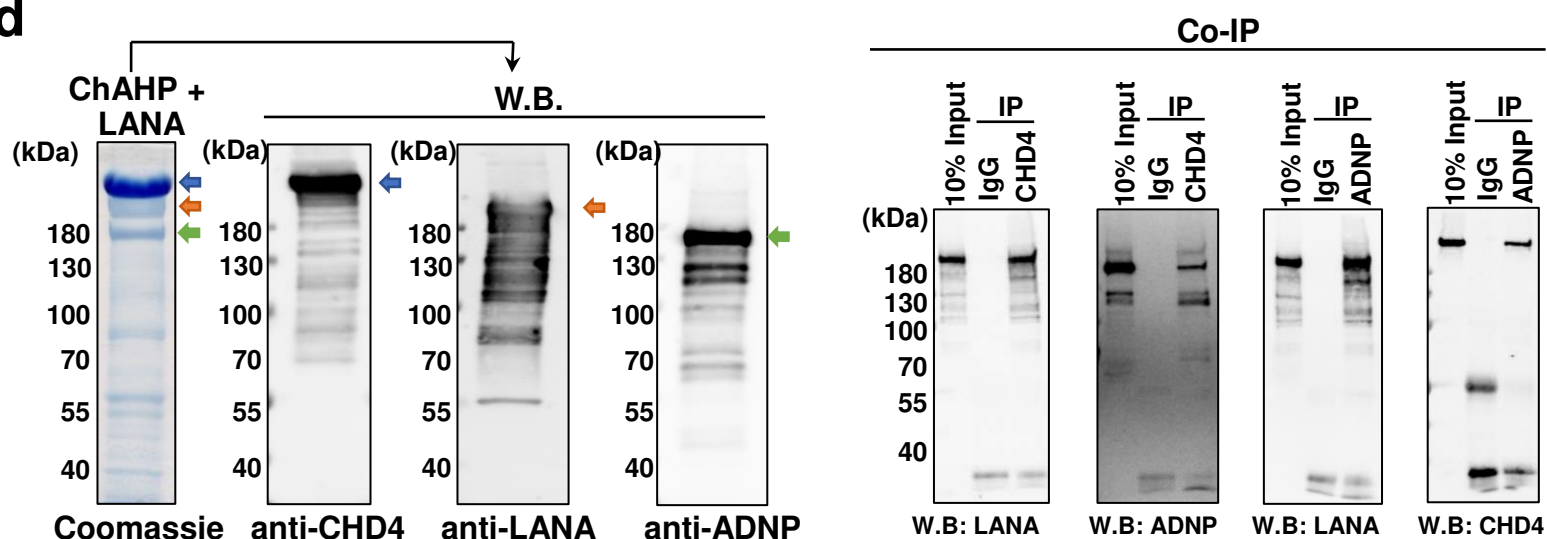
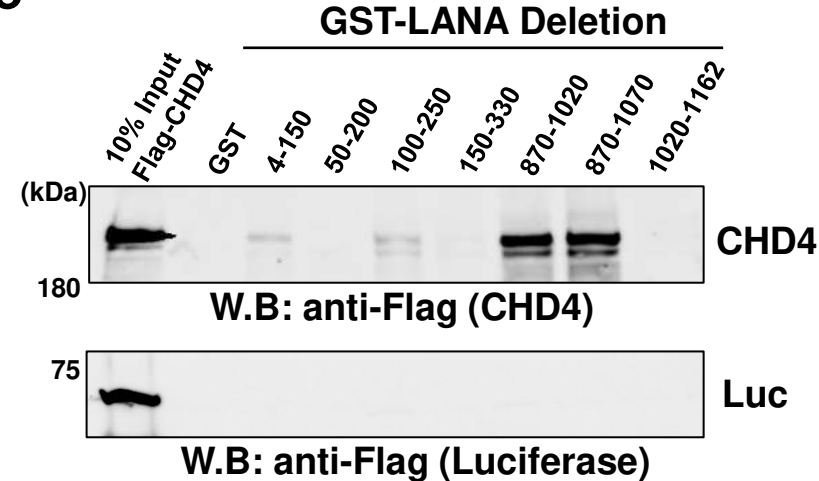
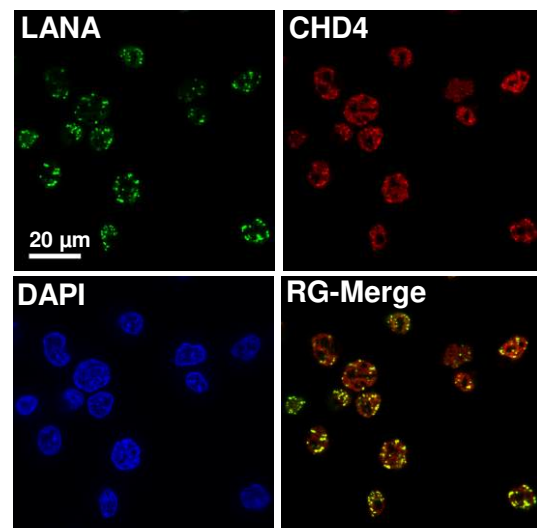
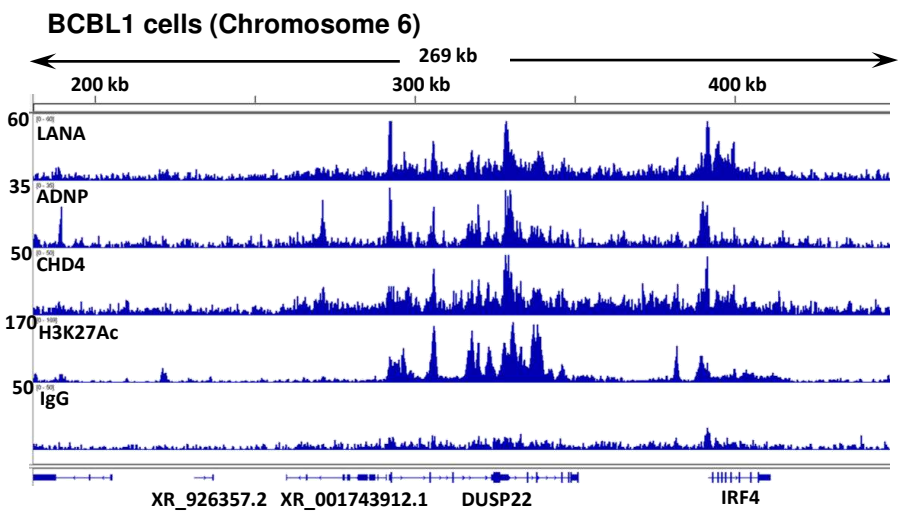
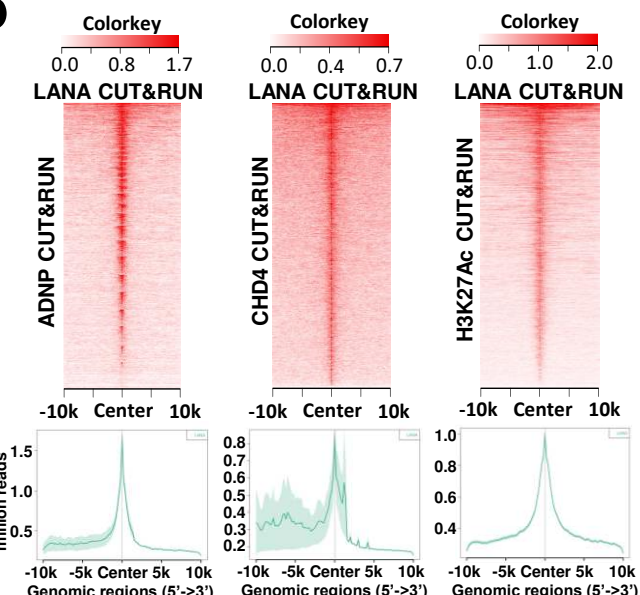
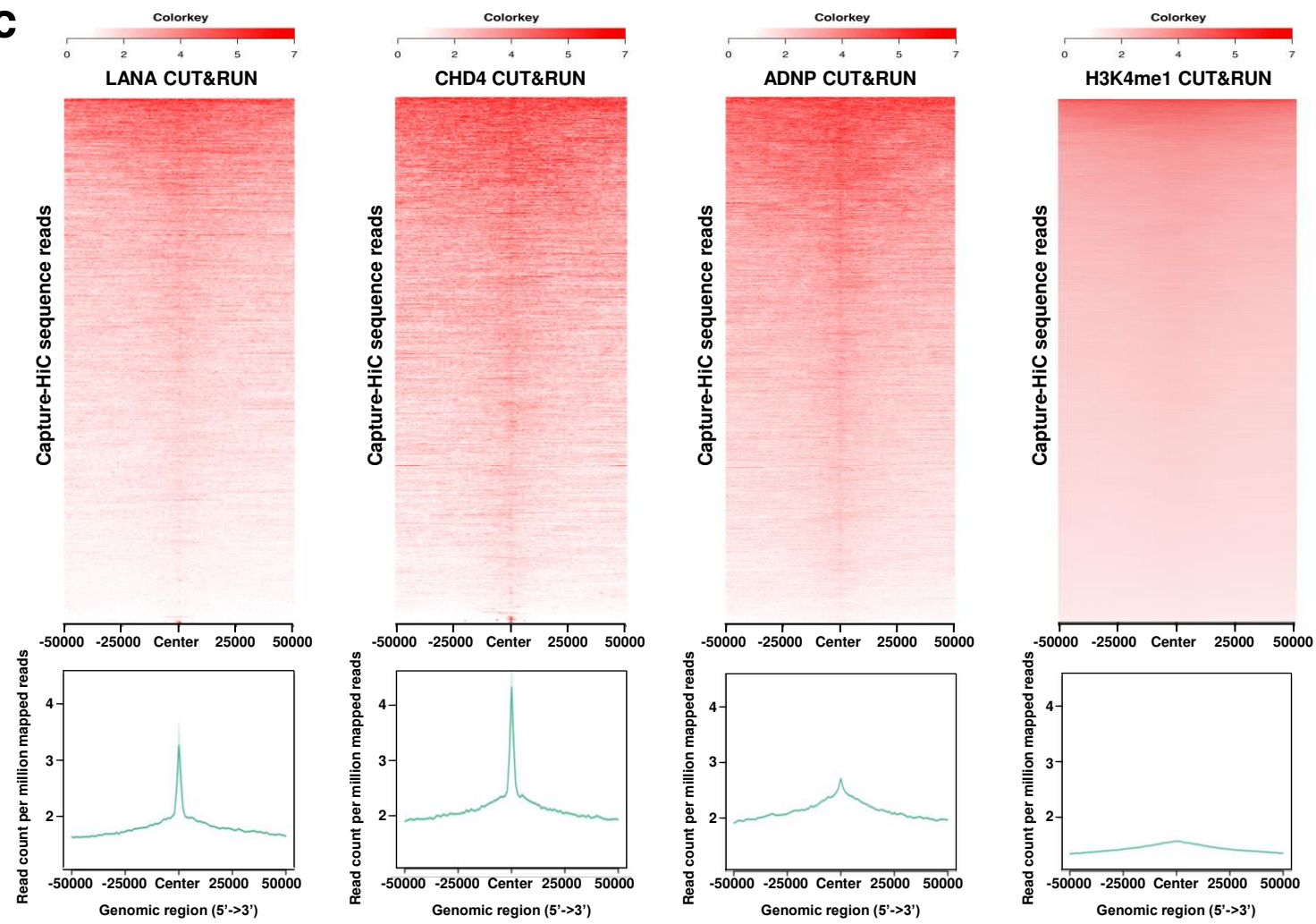
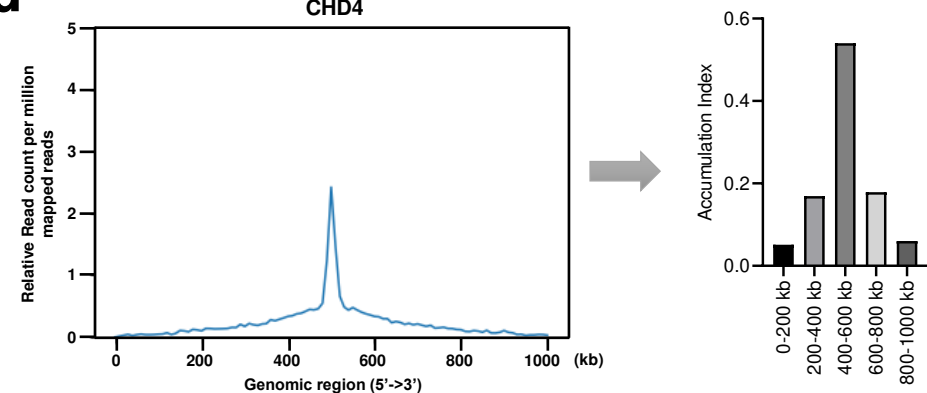
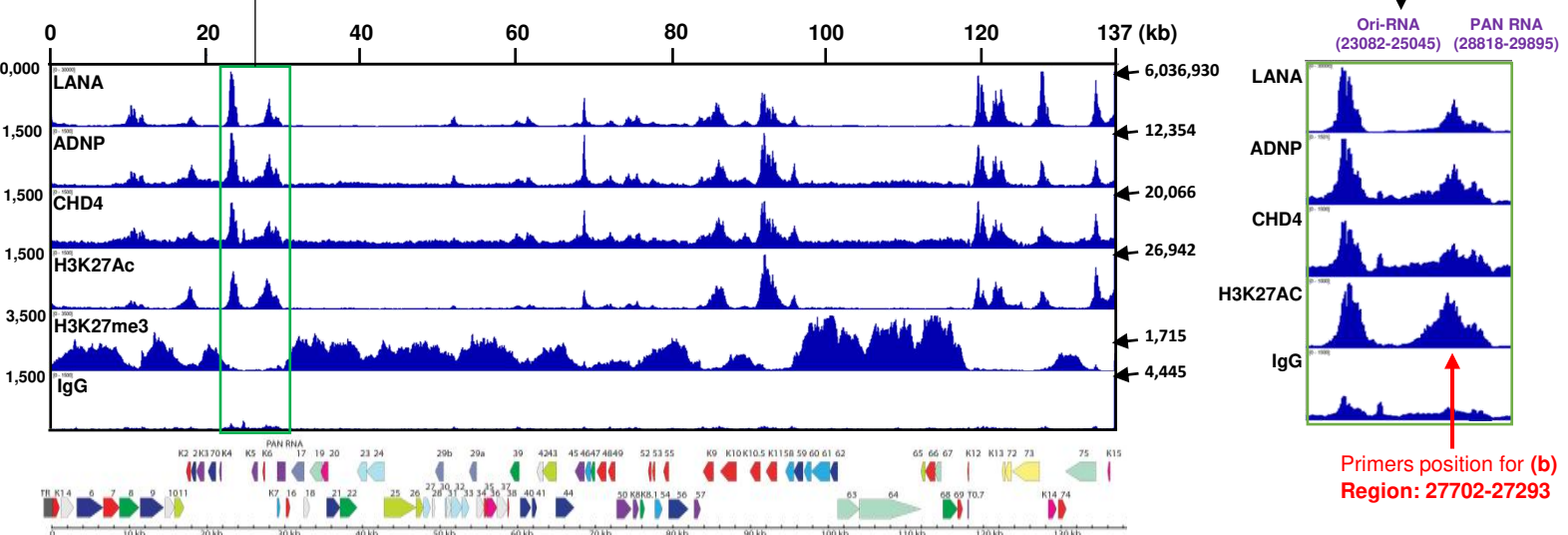
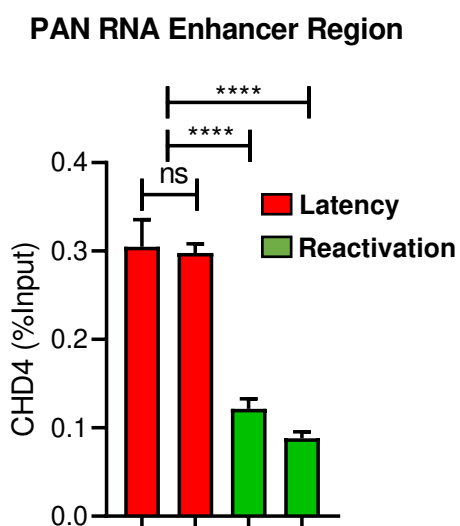
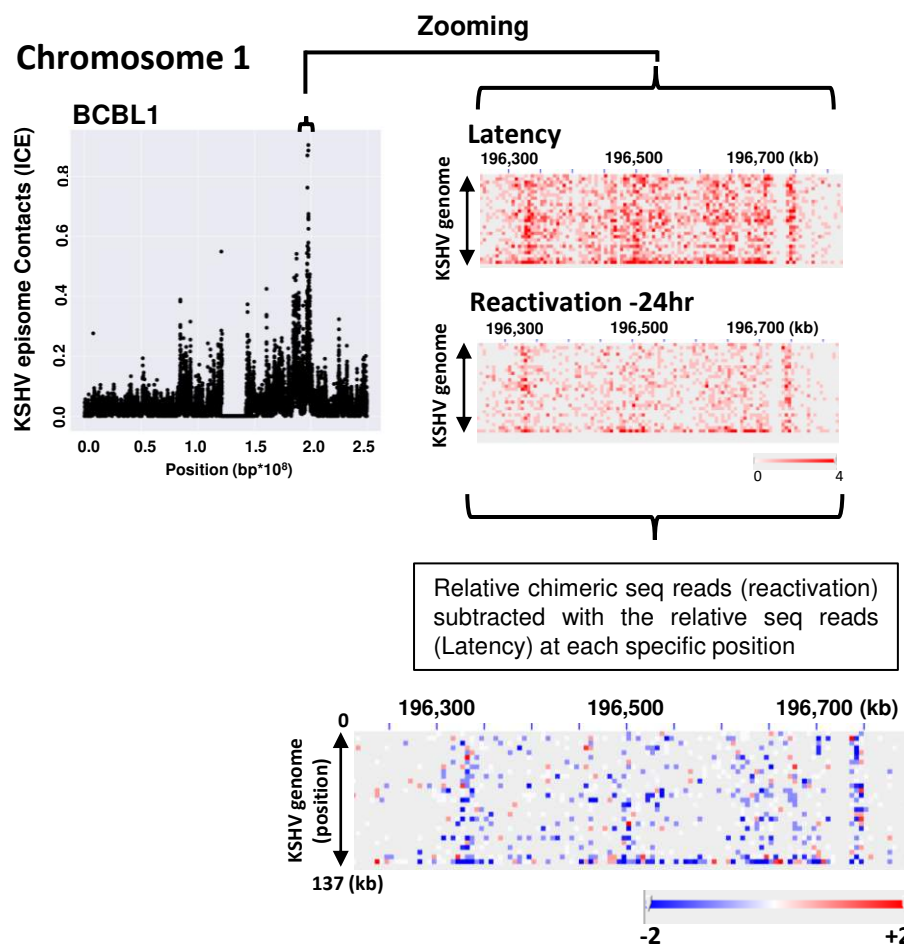
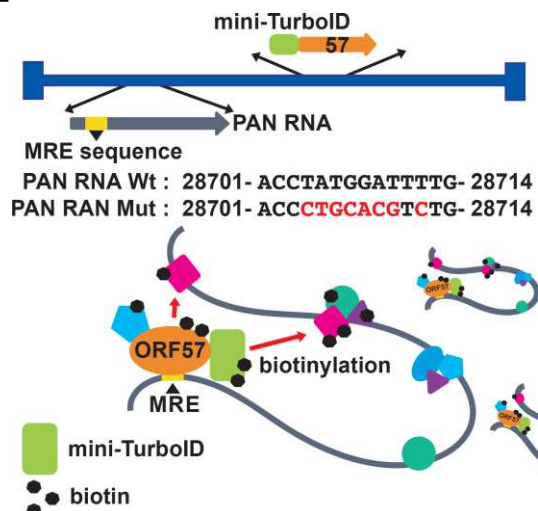
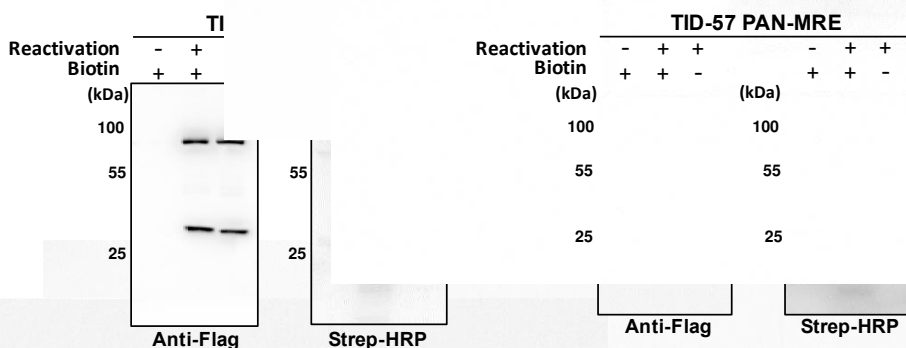
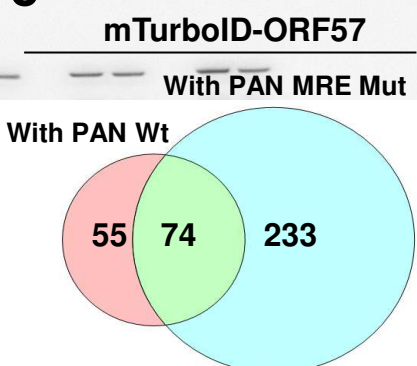


Fig. 1

a**b****c****d****e****f****Fig. 2**

a**b****c****d****Fig. 3**

a**b****c****Fig. 4**

a**b****c****d**

55 cellular proteins

GTF2F1	ZFR	C11orf58	DPYSL3
YAP1	FUBP1	RSRC2	CAD
STRAP	GPALPP1	CPSF1	NKRF
SARNP	PRPF4	YTHDF2	SCAF11
SLAIN2	SUB1	NELFE	KIF5B
FLII	WDR33	NCOR2	HNRNPL
EPS15	ABRAXAS2	DBNL	DHX8
IGBP1	RBM22	AKAP8	KNOP1
SEPTIN11	TACC2	ZCHC8	MIF
CLP1	PPFIA1	NSRP1	SRSF3
TAF7	NAT10	PGD	DIDO1
PPP1R2	EIF4B	ATAD3A	SNRPN
SLU7	ELOA	CHD4	MFAP1
SF1	GPATCH1	NCL	

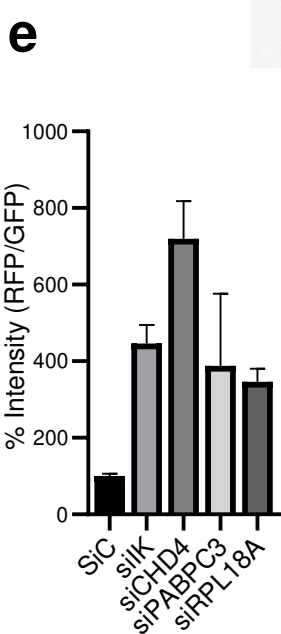
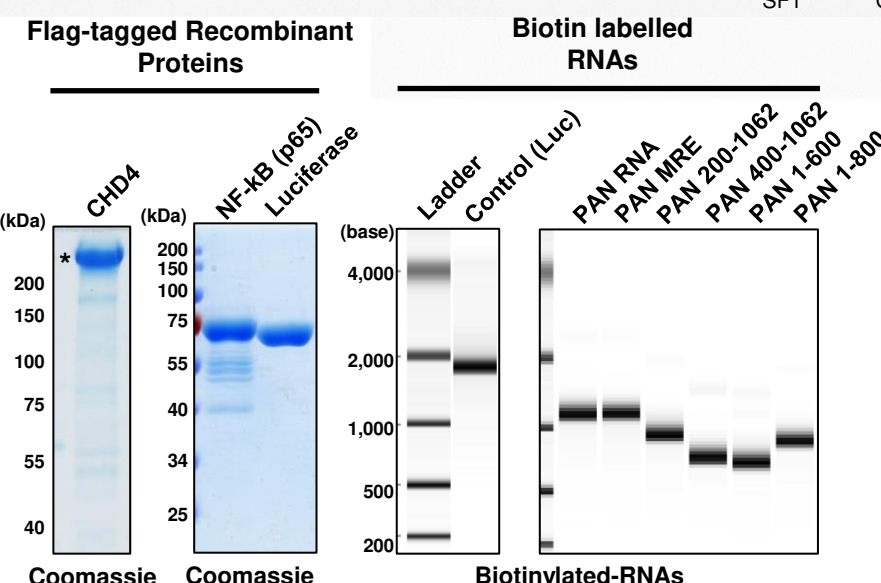
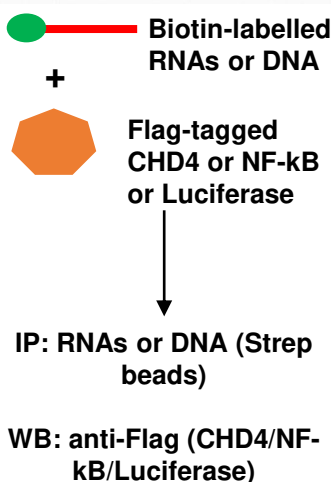
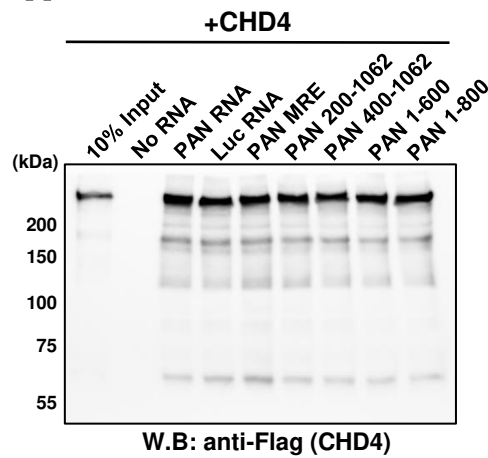
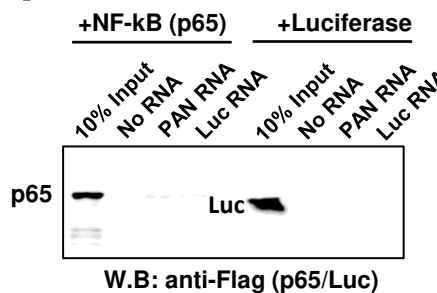
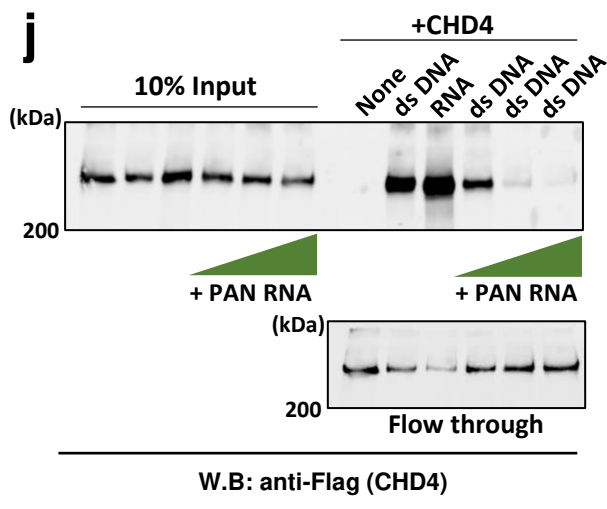
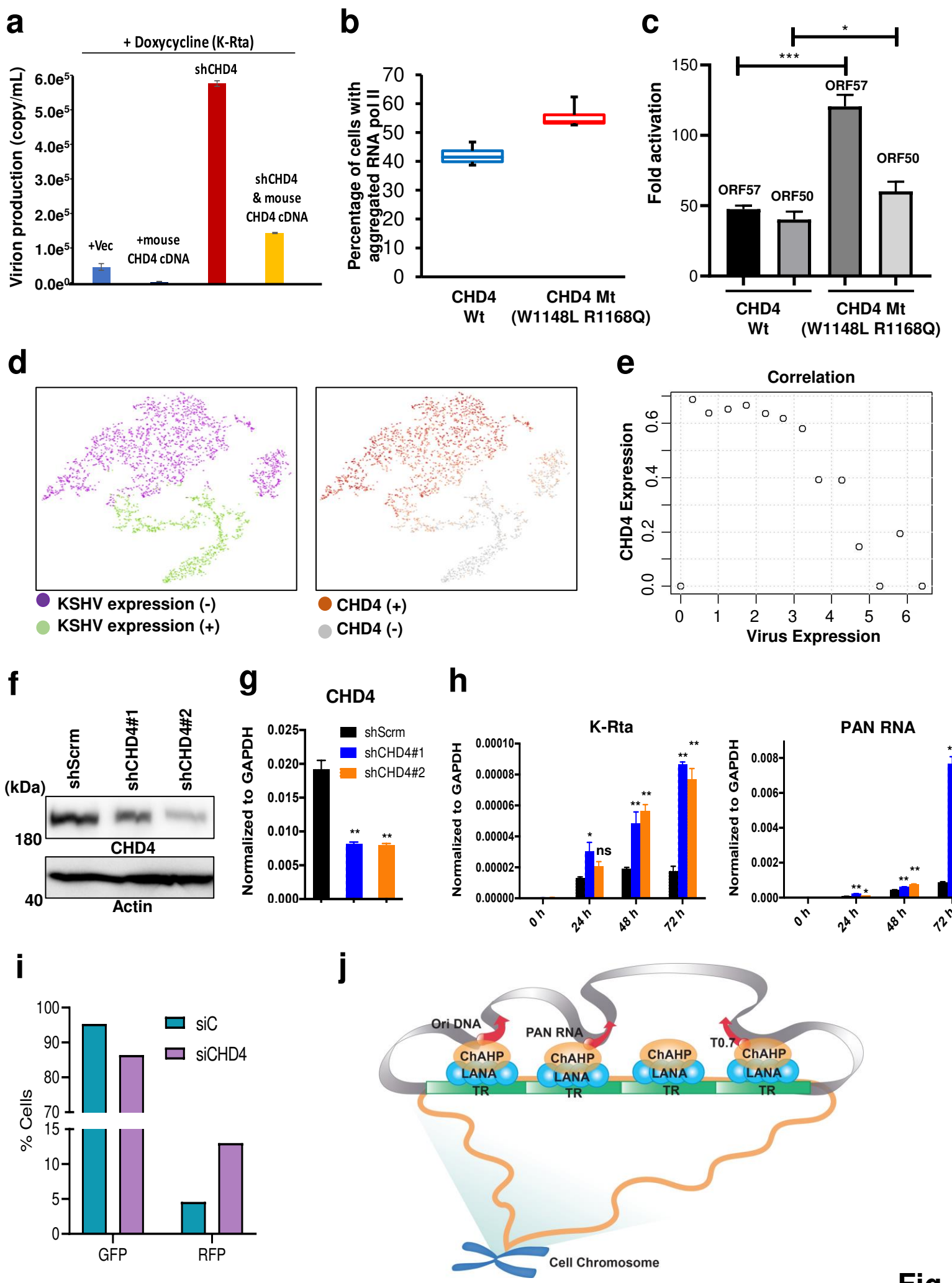
e**f****g****h****i****j**

Fig. 5



Figures

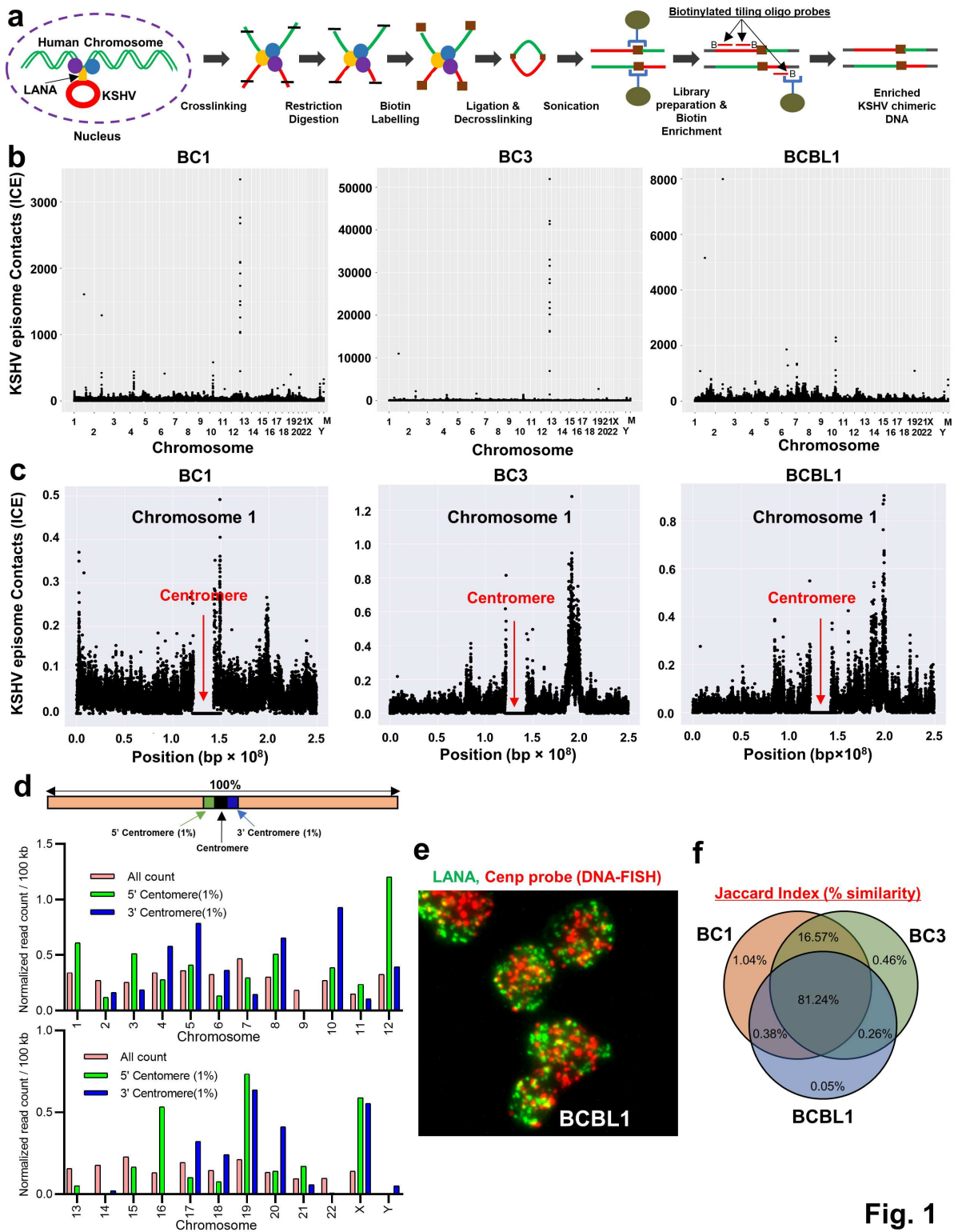


Fig. 1

Figure 1

Fig. 1 KSHV episome-tethering sites in KSHV positive cell lines. (a) Schematic workflow for Capture-HiC (CHi-C). (b) KSHV episome-docking sites on host cell chromosomes. CHi-C chimeric DNA ligation products composed of sequences derived from the KSHV and human genomes were mapped in three

naturally-infected PEL cells. For BCBL-1 cells, three biological replicates were performed with nearly identical results (similarity 0.95). M, mitochondrial chromosome. ICE-corrected profiles depicting sums of filtered read counts binned at 10 kb resolution are shown. (c) Selected chromosome 1 in zoomed view. Chromosome 1 dot plots were depicted, which displays enrichment of sequence reads near the centromere. Red arrows indicate the position of the centromere. Extended panels for all other individual chromosome for three cell lines are presented in Supplementary Fig. 1a-c. (d) KSHV episomes preferentially localize near the centromere. KSHV episode contacts were calculated in BCBL-1 cells for sequence reads in 1% (length of the respective chromosome) of the 5'-and 3'- centromere and compared with the average of the total chromosome read count. (e) LANA protein locates near the centromere. DNA-FISH was used to visualize the location of the centromere (red) and KSHV episomes were indirectly visualized by staining LANA dots (Green) in BCBL-1 cells. The centromere and LANA were probed using a Cenp probe and anti-LANA antibody respectively with IFA. The two signals were frequently co-localized, and 3D view and their image analyses are presented in Supplementary Fig. 2. (f) Jaccard statistics and Venn diagram. Venn diagram shows percent similarity of KSHV episode-tethering positions among BC-1, BC-3 and BCBL-1 cells.

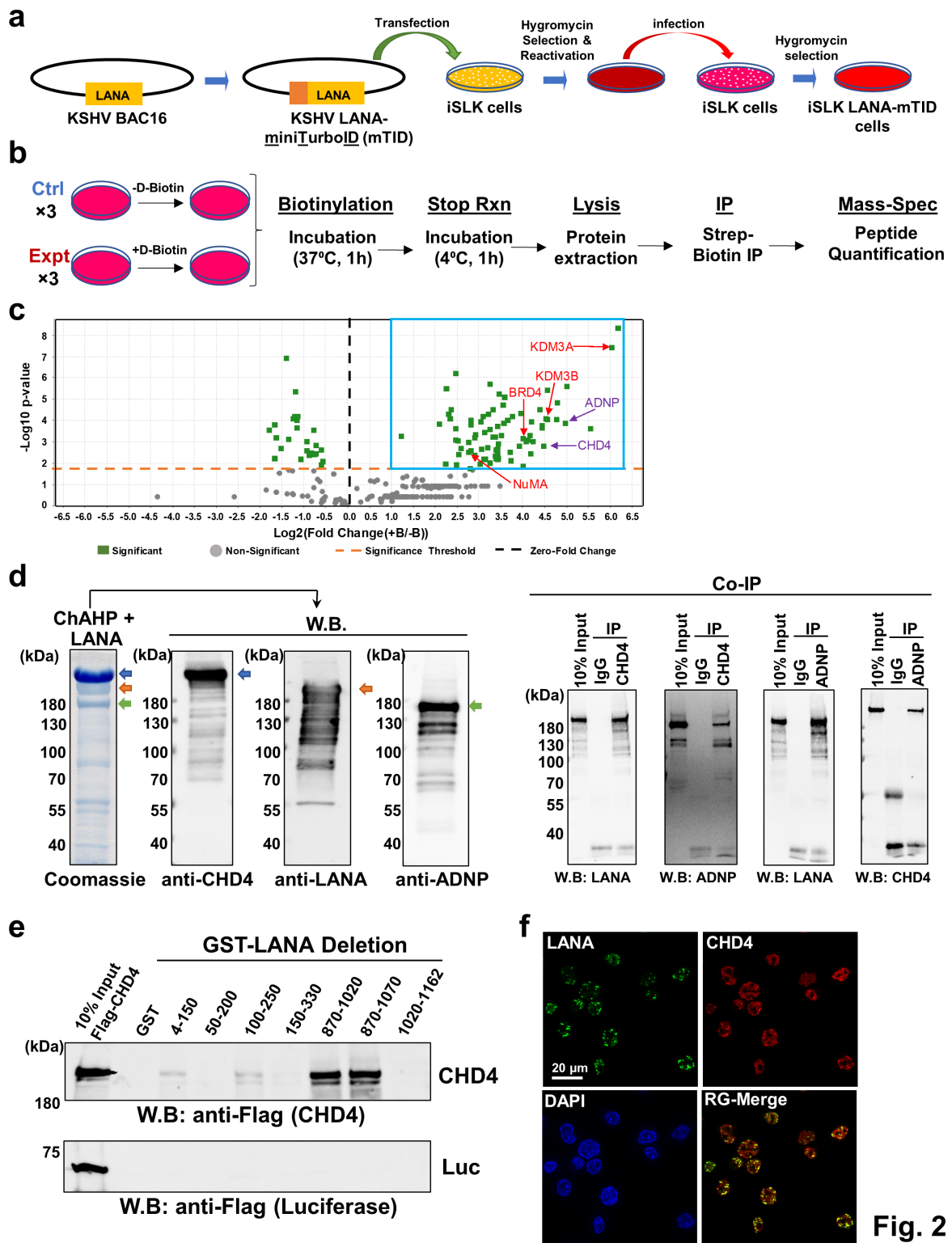


Fig. 2

LANA interacts with the ChAHP complex. (a) A schematic diagram of preparation of recombinant KSHV infected iSLK cells. A mini-TurboID (mTID) was fused to the N-terminus of the LANA open reading frame to generate KSHV LANA-mTID. KSHV LANA-mTID was transfected into iSLK cells followed by production of viral particles by stimulating cells with doxycycline (1 µg/ml) and sodium butyrate (3 mM) for 5 days. Virus was used to infect iSLK cells and cells were selected with hygromycin (1 mg/ml) to obtain an iSLK-

LANA mTID stable cell line. (b) Experimental design for preparing samples for protein ID. iSLK-LANA mTID cells were left un-incubated (-) or incubated (+) with D-Biotin (500 μ M) for 1 hr. Unincubated (-) cells were used as control samples. Each protein ID was performed in three biological replicates. (c) Volcano plot depicting proteins in close proximity to LANA. The volcano plot represents proteins identified in close proximity to LANA. Proteins with an abundance Log2 FC of greater than or equal to 1 and p-value less than 0.05 were selected and are shown by blue box. T-test was used for calculating the p-value. Purple color; ChAHP components. Red color; previously identified proteins as LANA interacting proteins. (d) LANA interacts with CHD4 and ADNP in vitro. LANA, CHD4 and ADNP complex, which consists of Flag-LANA (gold arrow), Flag-CHD4 (blue arrow), and His-ADNP (green arrow) was prepared by co-infected three recombinant baculoviruses, and the protein complex was isolated in the presence of 500 mM NaCl and 10% glycerol with affinity purification. The authenticity of respective protein band was confirmed by immunoblotting with specific antibodies. Coomassie staining is shown. An equimolar amount (100 nM) of the three proteins were incubated in binding buffer and immunoprecipitated with the specific antibodies of one another. Ten percent of the reaction before immunoprecipitation was shown as controls. W.B: Western Blotting, Co-IP: Co-immunoprecipitation. (e) CHD4 interaction site on LANA. Purified GST-tagged LANA deletions, Flag-tagged luciferase and 41 Flag-tagged CHD4 were prepared from recombinant baculovirus infected Sf9 cells. An equal amount (1 μ g) of each LANA deletion protein was incubated with full length Flag-tagged luciferase (1 μ g) or Flag-tagged CHD4 (1 μ g) in binding buffer and interaction was probed with anti-Flag antibody. LANA deletion proteins used for this GST-pull down assay are presented in 910 Supplementary Fig. 4. (f) LANA co-localizes with CHD4 in BCBL-1. CHD4 and LANA were 911 probed with anti-CHD4 rabbit monoclonal antibody and anti-LANA rat monoclonal antibody, 912 respectively. Images were taken with Keyence fluorescence microscopy. Scale bar (20 μ m) is 913 shown

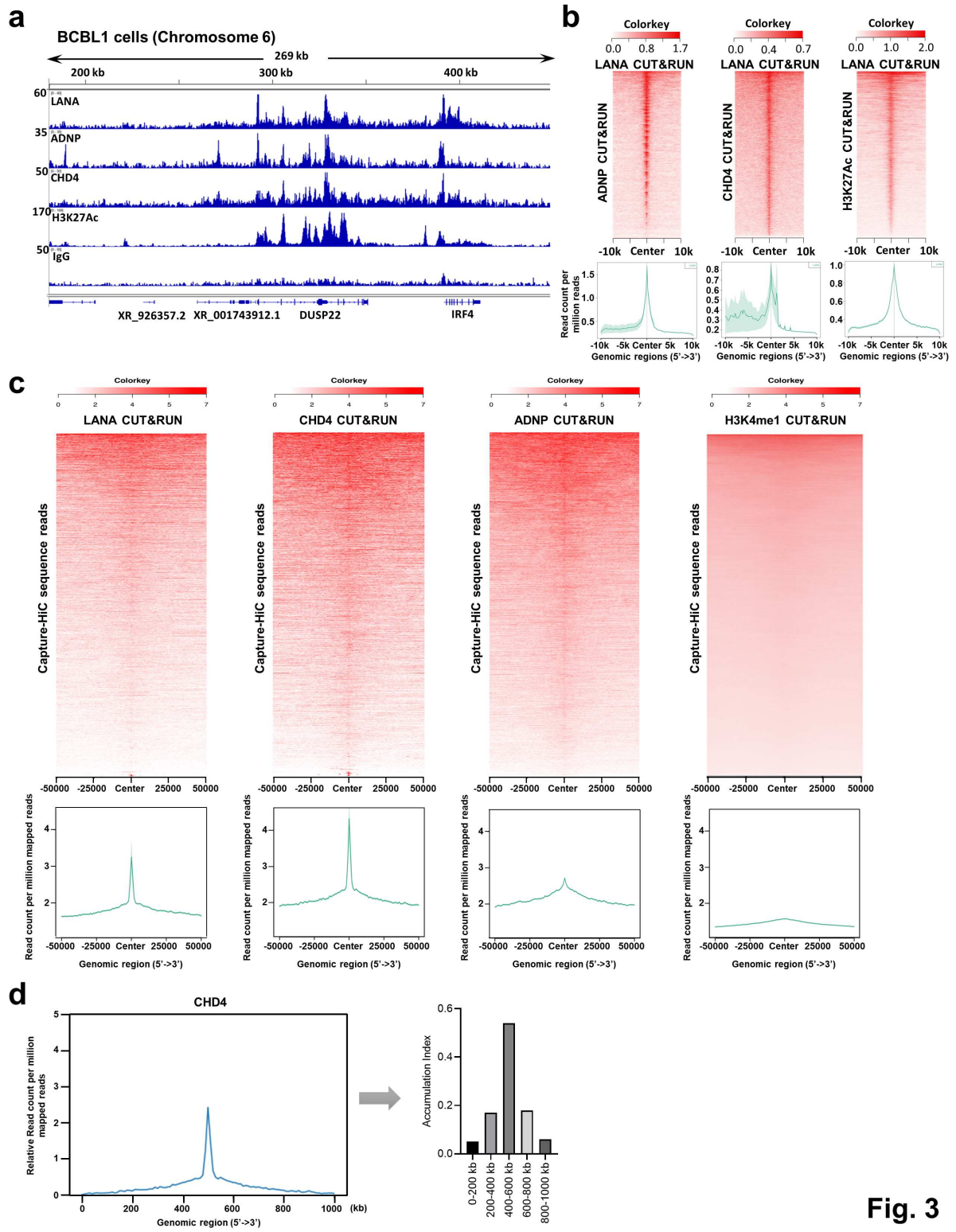


Fig. 3

Figure 3

Association of ChAHP complex binding with KSHV episome-tethering sites. (a) CUT&RUN analysis for LANA, ADNP, CHD4 and H3K27Ac. The indicated antibodies were used for CUT&RUN in BCBL-1 cells. CUT&RUN peaks were visualized with Integrative Genomics Viewer (IGV) and a snapshot of one of the major binding sites (IRF4 super enhancer region) is shown. The number on the left-hand side denotes the height of the peak (e.g., read depth) and the number along the top denotes the positions on chromosome

6. (b) Heatmaps for co-occupancies of LANA with ADNP, CHD4 and H3K27Ac on chromosomes. Heatmap (middle) and average profile (bottom) showing correlation of LANA enrichment (by color intensity and region) with ADNP, CHD4, and H3K27Ac occupancies. Average profile plot summarizing the heatmap (bottom). The lighter green shade represents the standard error (SEM) on the average profile plot. Color keys are shown on the each heatmap (top). (c) Heatmaps for correlation of CHi-C with CUT&RUN signals. The association between CHi-C chimeric reads and LANA, CHD4, ADNP and H3K4me1 CUT&RUN peaks were depicted as heatmap and average profile plot. (d) Accumulation index around CHD4 binding sites. The accumulation 42 of CHD4 is displayed as a proportion of area under the curve of the relative average profile. Association between distance from CHD4 summit peak and relative chimeric sequence counts is shown as a bar chart.

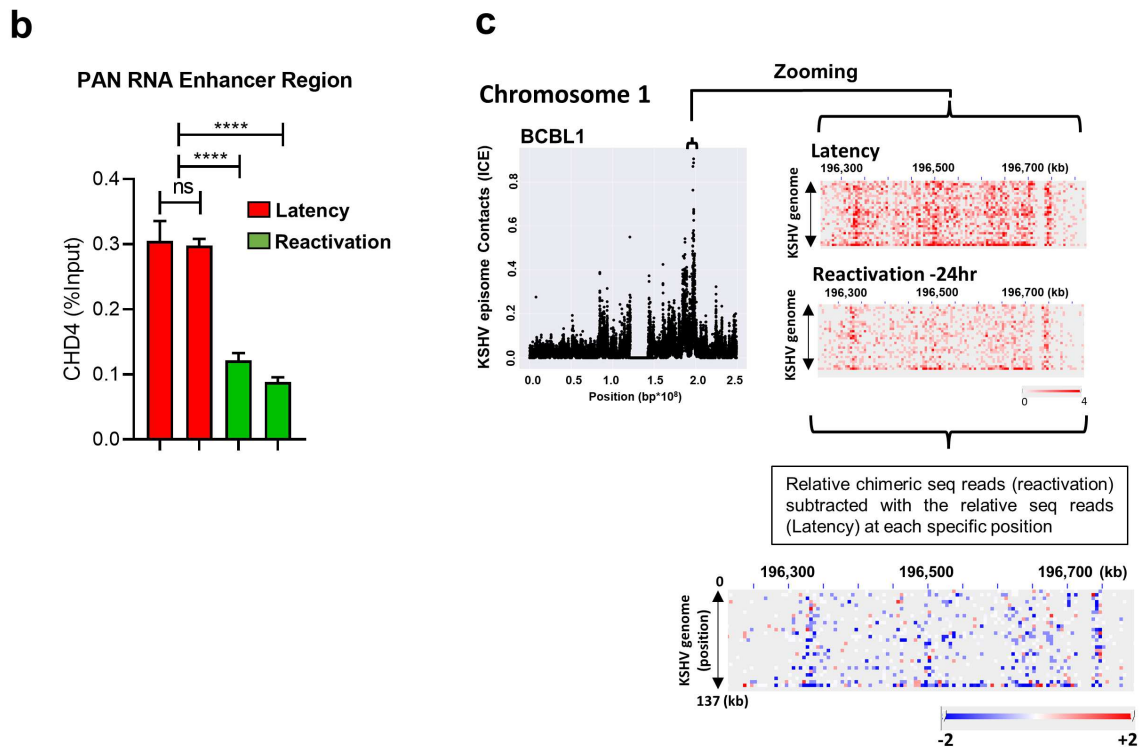
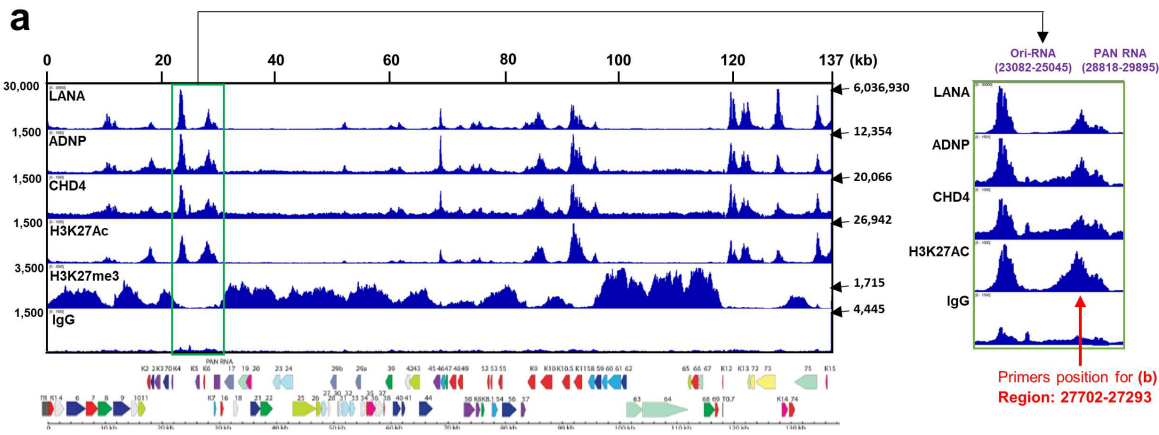


Fig. 4

Figure 4

LANA, CHD4 and ADNP colocalize on the KSHV genome. (a) CUT&RUN analysis. The indicated antibodies were used for CUT&RUN in BCBL-1 cells and sequence reads were mapped to the KSHV genome. An IGV snapshot and KSHV genome map are shown. The number on the left-hand side denotes the height of the peak (e.g., read depth), the number along the top denotes the position on KSHV genome in kilobase (kb) and the number on the right-hand side indicated by arrow denote the height of the peak on terminal

repeat region (TR). Selected region is zoomed in to show Ori-RNA and PAN RNA region. Primer used in Fig. 4b is also shown with red arrows and number show the exact location of the amplified region by the primers. (b) Regulation of CHD4 on the KSHV episome during reactivation. TREx-BCBL-1 cells were reactivated with doxycycline (1 μ g/ml) and sodium butyrate (3 mM) for 24 hrs. CUT&RUN was performed on un-reactivated (latency) and reactivated cells for CHD4. CHD4 binding on the PAN RNA promoter region (red arrow in Fig. 4a, right panel) was calculated relative to the input sample (n=3, two biological replicates are shown). (c) Detachment of KSHV episomes by reactivation. BCBL-1 cells were reactivated with doxycycline (1 μ g/ml) and TPA (20 nM) for 24 hrs. Chimeric sequence reads for un-reactivated (latency) and reactivated cells were mapped to the host chromosomes and visualized by Juicebox. Relative KSHV episome tethering during reactivation for the selected region on chromosome 1 was calculated by subtracting relative chimeric sequence reads in latency from relative chimeric sequence reads during reactivation. Blue and red dots indicate decreased and increased chimeric sequence reads respectively.

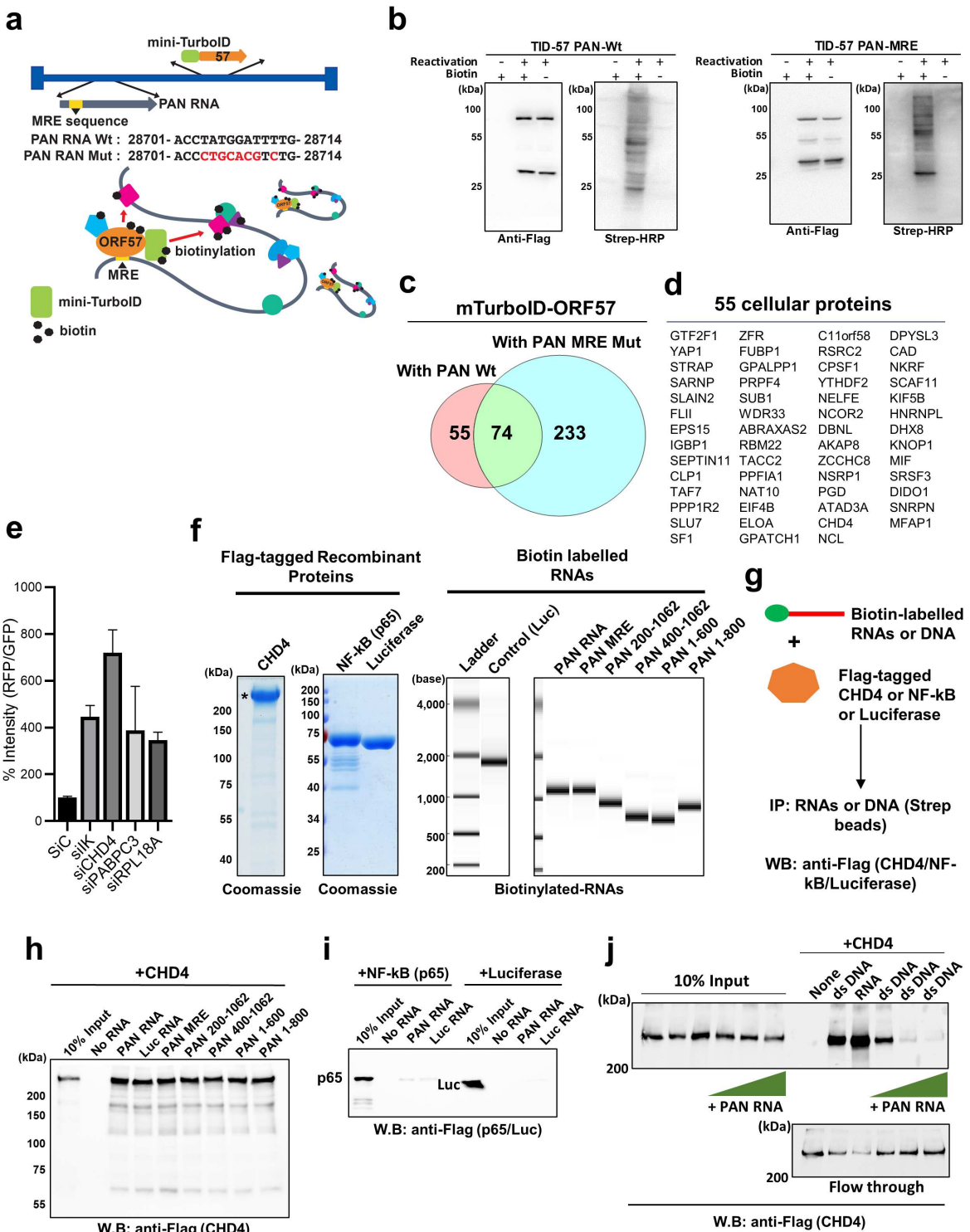


Fig. 5

Figure 5

CHD4 is both an RNA and DNA binding protein. (a) A schematic diagram of recombinant KSHVs. Mini-TurboID is fused to the N-terminus of ORF57 open reading frame and the ORF57 binding site (MRE) of PAN RNA was mutated as shown. (b) Immunoblotting. Recombinant KSHV infected iSLK cells (TID-57 PAN-Wt and -MRE) were either untreated or induced for reactivation with doxycycline (1 µg/ml) and TPA (20 nM) for 24 hrs. Blots were probed with either anti-Flag antibody (for mini-TurboID-ORF57) or

Streptavidin-HRP (for biotinylated proteins). (c) Venn diagram. The Venn diagram indicates the number of identified proteins with a P value less than 0.05. Each protein ID was performed in three biological replicates. (d) PAN RNA-mediated interacting proteins with ORF57. The proteins found enriched in PAN RNA962 WT samples are shown. The entire list of proteins and peptide counts are presented in Supplementary Table 2. (e) siRNA screening with KSHV reactivation as readout. Recombinant KSHV reactivation, which encodes RFP under control of the PAN RNA promoter, was used to screen the effects of KSHV reactivation. RFP signal intensity was measured with Image J, and the GFP signal was used as internal controls. Three randomly selected fields in the middle of each well were quantified and the average intensity was plotted. (f) Recombinant proteins and synthesized PAN RNAs. Recombinant Flag-tagged proteins were expressed with baculovirus and purified with Flag-agarose beads. Coomassie staining of Flag-CHD4, Flag-NF970 kB (p65), and Flag-luciferase used for pull-down studies are shown. (g) Schematic for in vitro interaction assay performed in Fig. 5 (h-j). (h) CHD4 binds RNAs in a sequence972 independent manner. RNA pull-down was performed with the indicated biotinylated PAN RNA deletions, mutation (MRE), and irrelevant RNA (luciferase mRNA), and interaction was probed by immunoblotting with anti-Flag antibody. Beads alone (No RNA) was used for background 44 control. (i) RNA pull down was performed with indicated biotinylated RNAs, and p65 and Luciferase (Luc) were visualized by using anti-Flag antibody. (j) PAN RNA competes with CHD4 DNA binding. Pull-down analyses with biotinylated ssRNA or dsDNA was performed. CHD4 (100 nM) was incubated with biotinylated RNA (100 nM) or biotinylated dsDNA (100 nM) in 40 μ L binding buffer. Increasing amounts of non-biotinylated PAN RNA at 1:1, 1:10, and 1:20 (dsDNA vs. ssRNA) were also incubated, and precipitated CHD4 protein in the pull-down was probed with anti-Flag antibody. Flow-through and 10% of the input reaction before pull-down were used as control.

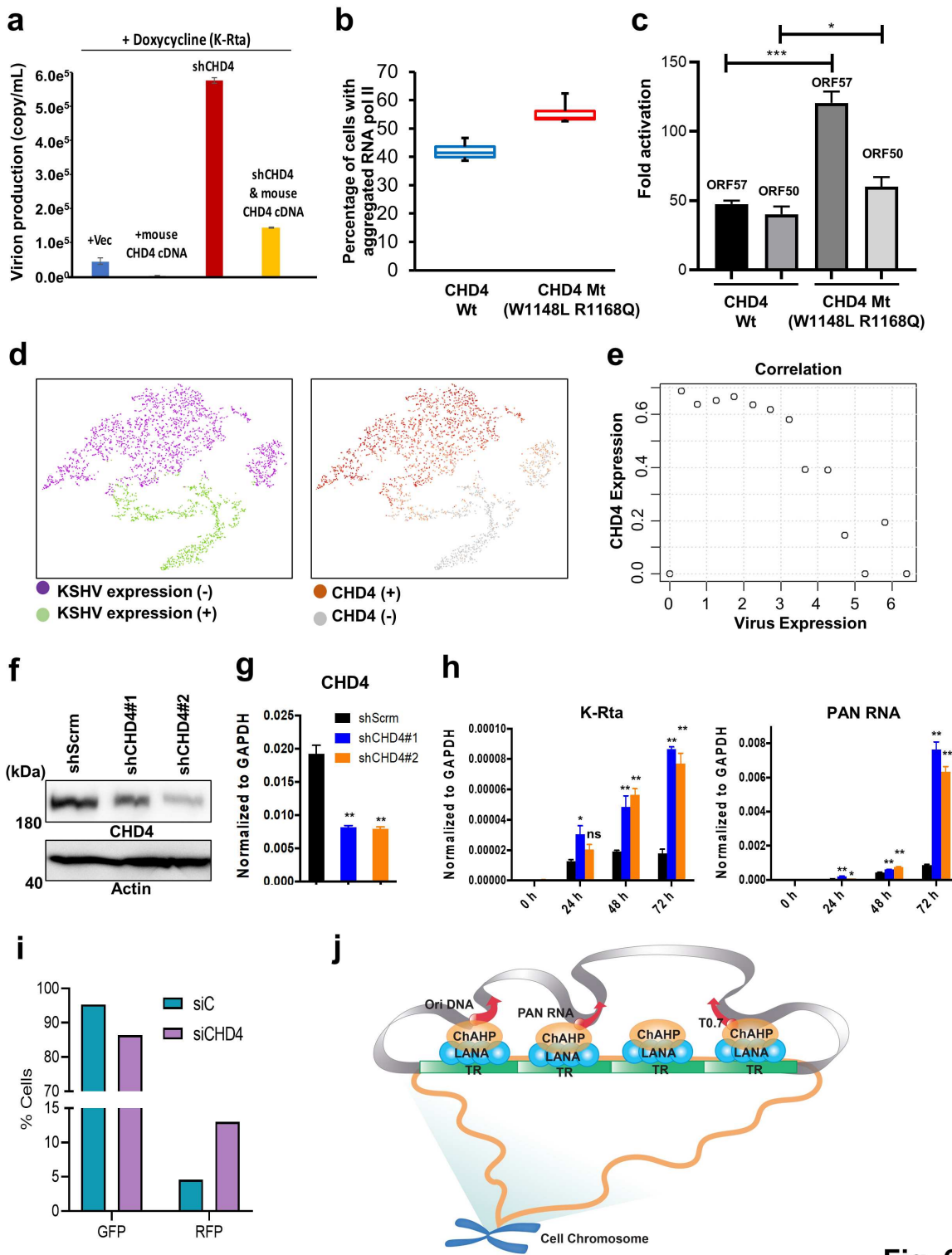


Fig. 6

Figure 6

CHD4 is important for latency maintenance and establishment. (a) CHD4 overexpression, knockdown and complementation. The iSLK.219 cell line was transfected with empty vector (Vec) or mouse CHD4 cDNA or human CHD4 shRNA, or CHD4 shRNA and mouse CHD4 cDNA for 48 hrs followed by KSHV reactivation with doxycycline (1 µg/ml) for 5 days. Encapsidated KSHV genomes in the culture supernatants were measured by qPCR to assess effects of CHD4 overexpression or knockdown on KSHV

reactivation. (b) CHD4 ATPase activity is important for prevention of nuclear aggregate formation. iSLK cells latently infected with BAC16-Wt was transfected with Flag-tagged mouse wild type CHD4, or an ATPase domain mutant was transfected and stained with anti-Flag. Transcriptional factory formation was assessed by staining RNAII. The percentage of aggregate formation in Flag-positive cells was measured and plotted. Three biological replicates were performed, and 50 cells were counted in each of the three biological replicates. (c) CHD4 ATPase activity is important for inhibiting viral gene expression during reactivation. iSLK.219 cells were transduced with an equal amount of CHD4 wild type (wt) and CHD4 mutant (mt) lentivirus for 2 days. Cells were 45 reactivated with doxycycline (1 µg/ml) for 2 days and ORF50 and ORF57 gene expression was quantified by RT-qPCR. Untreated cells were used for calculating the relative expression of ORF50 and ORF57. GAPDH was used as a negative control. *p<0.05, ***p<0.001 (comparing with CHD4 Wt). (d-e) Single cell sequencing. iSLK.219 cells were reactivated by induction of K-Rta expression from doxycycline inducible promoter for 24 hrs. Single-cell sequencing was performed with the 10x Genomics platform. A cell suspension was prepared followed by cell partitioning and 3' cDNA synthesis on the Chromium Controller and dual-index library preparation with 10x Genomics kitted reagents. (d) tSNE. tSNE was applied to separate cell clusters and KSHV gene (d, left panel) and CHD4 (d, right panel) expressing cells were marked. (e) Negative correlation between CHD4 and viral gene expression. Cells were divided into groups based on the amount of KSHV transcripts. A table and distribution of cell numbers and amount of KSHV transcripts are shown in Supplementary Fig. 6a-b. Intervals used to separate cell groups are also listed in Supplementary Fig. 6b. A correlation was established based on CHD4 expression in different groups of KSHV transcripts. (f-h) CHD4 knockdown and KSHV lytic gene expression during de novo infection. 293T cells were transduced with scramble shRNA (shScrm) or shCHD4 and stably selected with antibiotic. Immunoblot (f) and RT-qPCR (g) analysis of CHD4 in the 293T stable cell lines are shown. 293T stable cells were infected with rKSHV.219 for 24 hrs and total RNA was harvested at the indicated time points. (h) K-Rta and PAN RNA, was measured by RT-qPCR and normalized to GAPDH. *p<0.05, **p<0.01 (comparing with shScrm). (i) Flow cytometry. 293T cells were transfected with control siRNA (siC) or CHD4 siRNA (siCHD4) for 48 hrs followed by infection with rKSHV.219 virus for 96 hrs. Flow cytometry analysis was performed to calculate the number of GFP- and RFP-positive cells in siC and siCHD4 knockdown cells. (j) KSHV latency model with ChAHP. KSHV episomes 46 tether at epigenetically active regions with the ChAHP complex, and TR-loaded LANA/ChAHP prevents robust viral lncRNA expression. The action of robust lncRNA expression in lytic KSHV infection functions as an enhancer for viral ORFs that are physically neighboring with lncRNA genomic regions. Stimulation of K-Rta, in part by decreased CHD4 expression, triggers robust PAN RNA expression in the presence of ORF57, which competes with CHD4 DNA binding to enhance KSHV reactivation and detach KSHV episomes from CHD4-enriched host chromosome regions.

Supplementary Files

This is a list of supplementary files associated with this preprint. Click to download.

- [SupplementaryFigures.pdf](#)

- SupplementaryTable1.xls
- SupplementaryTable2.xls
- SupplementaryTable3.xls